Brachialactone isomers and derivatives of Brachiaria humidicola reveal contrasting nitrification inhibiting activity

Citation:

Egenolf, K.; Conrad, J.; Schöne, J.; Braunberger, C.; Beifuß, U.; Walkerc, F.; Nuñez, J.; Arango, J.; Karwata, H.; Cadisch, G.; Neumanne, G.; Rasche, F. (2020) Brachialactone isomers and derivatives of Brachiaria humidicola reveal contrasting nitrification inhibiting activity. Plant Physiology and Biochemistry 154 p. 491-497. ISSN: 0981-9428

Publisher's DOI:

https://doi.org/10.1016/j.plaphy.2020.06.004

Access through CIAT Research Online:

https://hdl.handle.net/10568/108784

Brachialactone isomers and derivatives of *Brachiaria humidicola* reveal contrasting nitrification inhibiting activity

Konrad Egenolf[a,d], Jürgen Conrad[b], Jochen Schöne[c], Christina Braunberger[b], Uwe Beifuß[b], Frank Walker[c], Jonathan Nuñez[d,1], Jacobo Arango[d], Hannes Karwat[a,d,2], Georg Cadisch[a], Günter Neumann[e], Frank Rasche[a*]

[a]Institute of Agricultural Sciences in the Tropics (Hans-Ruthenberg-Institute), University of Hohenheim, 70593 Stuttgart, Germany

[b]Institute of Chemistry, University of Hohenheim, 70593 Stuttgart, Germany

[c]Institute of Phytomedicine, University of Hohenheim, 70593 Stuttgart, Germany

[d] The Alliance of Bioversity International and the International Center for Tropical Agriculture (CIAT), Km 17 Recta Cali-Palmira, A.A. 6713, Cali, Colombia

[e]Institute of Crop Sciences, University of Hohenheim, 70593 Stuttgart, Germany

[1]Present address: Manaaki Whenua – Landcare Research, PO Box 69040, Lincoln 7640, New Zealand

[2]Present address: Centro Internacional de Mejoramiento de Maíz y Trigo (CIMMYT), Km 45 Carretera México-Veracruz, Col. El Batán, Texcoco, Edo. de Mexico 56130, Mexico

***Corresponding author:**

Dr. Frank Rasche

Phone: +49 (0) 711 459 24137

Fax: +49 (0) 711 459 22304

Email: frank.rasche@uni-hohenheim.de

Graphical Abstract

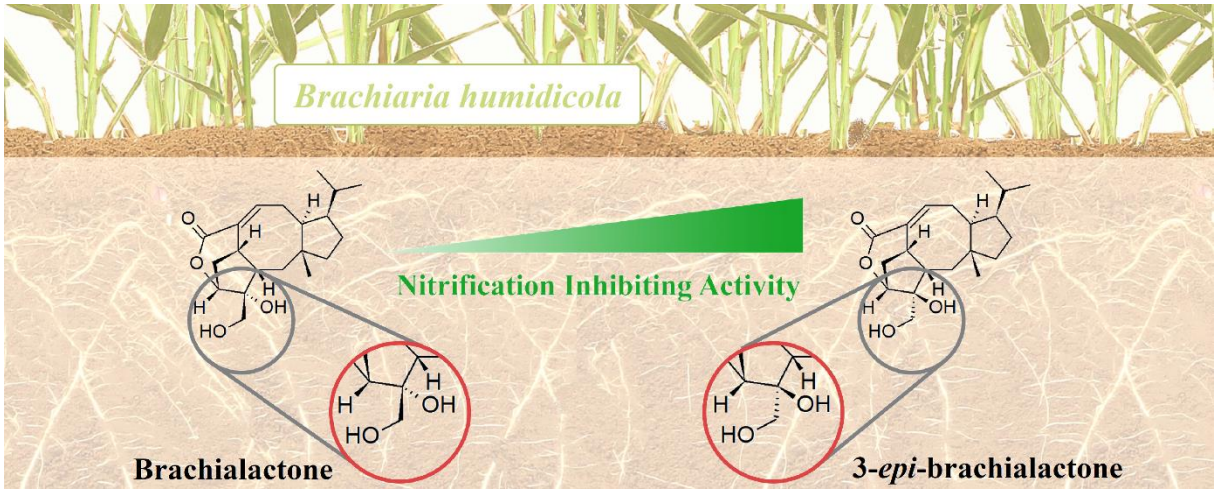

Abstract

Biological Nitrification Inhibition (BNI) of *Brachiaria humidicola* has been mainly attributed to the root-exuded fusicoccane-type diterpene brachialactone. We hypothesized, however, that according to the high diversity of fusicoccanes described for plants and microorganisms, BNI of *B. humidicola* is caused by an assemblage of bioactive fusicoccanes. *B. humidicola* root exudates were collected hydroponically and compounds isolated by semi-preparative HPLC. Chemical structures were revealed by spectroscopic techniques, including HRMS as well as 1D and 2D NMR. Nitrification inhibiting (NI) potential of isolated compounds was evaluated by a *Nitrosomonas europaea* based bioassay. Besides the previously described brachialactone (**1**), root exudates contained 3-*epi*-brachialactone (**2**), the C3-epimer of **1** (*m/z* 334), as well as 16-hydroxy-3-*epi*-brachialactone (**3**) with an additional hydroxyl group at C16 (*m/z* 350) and 3,18-epoxy-9-hydroxy-4,7-*seco*-brachialactone (**4**), which is a ring opened brachialactone derivative with a 3,18 epoxide ring and a hydroxyl group at C9 (*m/z* 332). The 3-*epi*-brachialactone (**2**) showed highest NI activity (ED_{50} ~ 20 µg mL^{-1}, ED_{80} ~ 40 µg mL^{-1}), followed by compound **4** with intermediate (ED_{50} ~ 40 µg mL^{-1}), brachialactone (**1**) with low and compound **3** without activity. In coherence with previous reports on fusicoccanes, stereochemistry at C3 was of high relevance for the biological activity (NI potential) of brachialactones.

Keywords: *Brachiaria humidicola*; Poaceae; BNI (Biological Nitrification Inhibition); forages; tropical savannas; *Nitrosomonas europaea*; fusicoccanes

1. Introduction

Nitrification – the microbial conversion of ammonium (NH_4^+) to nitrate (NO_3^-) – increases the mobility, thus availability of the soil mineral nitrogen (N) pool. This favors plant supply with N in the short-term but implies potential N losses in the form of NO_3^- leaching as well as denitrification derived gaseous N emissions in the long run (Coskun et al., 2017). Nutrient cycling in natural environments is proposed to rely on ecosystem self-regulation (Bardgett and McAlister, 1999) and it is argued that any self-regulating mechanism curbing N leakage at the ecosystem level should prevail in the course of evolution. In this respect, temperate forests evolved reduced N mobilization (mineralization, nitrification) rates and/or increased N immobilization capacities (Lodhi and Killingbeck, 1980; Robertson and Vitousek, 1981; Stark and Hart, 1997). In the case of African savannas, origin of both *Brachiaria* spp. and *Hyparrhenia* spp., it has been suggested that reduced net nitrification evolved as a plausible natural strategy to mitigate major N losses (Theron, 1951; Sylvester-Bradley et al., 1988; Lata et al., 2004).

Low net nitrification rates have mostly been attributed to reduced gross nitrification, as induced by allelopathic, plant exerted inhibition of soil nitrifier activity (Rice and Pancholy, 1972; Sylvester-Bradley et al., 1988). Accordingly, Subbarao et al. (2006) introduced the ecological concept of *Biological Nitrification Inhibition* (BNI), being defined as the allelopathic inhibition of soil nitrifier activity through the synthesis and release of nitrification inhibitors (NIs) by plants. This concept was corroborated by the successful isolation and molecular identification of several bioactive NIs from the tropical forage grass *Brachiaria humidicola* (Rendle) Schweick, Poaceae. Besides different NIs encountered in root (methyl-p-coumarate, methyl ferulate) and shoot (linoleic acid, α-linolenic acid) tissues of *B. humidicola* (Gopalakrishnan et al., 2007; Subbarao et al., 2008), nitrification inhibiting activity was specifically described for the fusicoccane-type tetracyclic diterpene brachialactone (Subbarao et al., 2009). Brachialactone was shown to be released into the rhizosphere in dependence of NH_4^+

availability and hence proposed to play a dominant role in nitrification inhibition of *B. humidicola*. Subbarao et al. (2009) concluded that brachialactone is responsible for up to 90% of the BNI potential in *B. humidicola*. The *in vitro* inhibition of chemoautotrophic ammonia (NH_3) oxidizing bacteria demonstrated by Subbarao et al. (2009) was proposed to be based on the interference of brachialactone with ammonia monooxygenase (AMO) and hydroxylamine oxidoreductase (HAO) pathways, the two key enzymes involved in the conversion of ammonia (NH_3) to nitrite (NO_2^-) (Hooper et al., 1997; Arp and Stein, 2003). The experimental evidence for this concept remains, however, elusive.

Uncertainty exists if brachialactone is the only fusicoccane-type bioactive NI produced by *B. humidicola*. It could be speculated that the general BNI potential of *B. humidicola* is rather based on an assemblage of NIs. Generally, the molecular description of new fusicoccanes often results in the discovery of related isomers and derivatives produced by the same organism (Muromtsev et al., 1994; de Boer and de Vries-van Leeuwen, 2012). Likewise, it has been suggested that different brachialactone forms may exist (G. Subbarao, personal communication). Moreover, it has been shown that the biological activity of fusicoccanes is highly dependent on the substituents at C3, C8 and C9 and their stereochemistry (Ballio et al., 1991; Sassa et al., 2002). To fully understand the functional relevance of brachialactone for nitrification inhibition of *B. humidicola*, a thorough investigation of possible isomerism and its implication for the biological activity of brachialactone is justified. The objective of the presented study was to screen *B. humidicola* root exudates for brachialactone and potential isomers / derivatives, including the description of their molecular structure. This analysis was complemented by the evaluation of selected root exudate fractions for their nitrification inhibiting activity.

2. Material and Methods

2.1. Root exudate collection in hydroponic system

Root exudate collection was performed on *Brachiaria humidicola* cv. CIAT 679 (commercial name "Tully"). This genotype has been extensively studied by the International Center for Tropical Agriculture (CIAT) and was ranked as a genotype with high BNI potential (Byrnes et al. 2017, Karwat et al. 2018). Plants were grown and root exudates were collected in a growth chamber based hydroponic system with a day length of 12 h, light intensity of 525 W m^{-2}, air humidity of 75 % and day/night temperatures of 30/20°C. The nutrient solution contained [µM]: NH_4NO_3 1200, KNO_3 400, $Ca(NO_3)_2$ 400, HNO_3 600, K_2HPO_4 200, $MgSO_4$ 200, $MgCl_2$ 100, Na_2SiO_3 200, FeNa-EDTA 50, H_3BO_3 10.0, $MnSO_4$ 4.0, $ZnSO_4$ 4.0, $CuSO_4$ 1.0, Na_2MoO_4 1.0. Resulting nutrient concentration were [µM]: N 4200, P 200, K 800, Ca 400, Mg 300, S 200, Si 200, Na 400, Cl 200, Fe 50, B 10.0, Mn 4.0, Zn 4.0, Cu 1.0, Mo 1.0 and pH of the nutrient solution was 4.8.

Plants of *B. humidicola* were propagated vegetatively through cuttings and cultivated over a period of 6 weeks at a density of 36 plants per 18 L of nutrient solution. The nutrient solution was replaced every 2-3 days. Thereafter, exudate collection was performed into fresh nutrient solution with 4 plants L^{-1} of nutrient solution during 24 h. After root exudate collection, the nutrient solution was filtered to remove root debris. Organic compounds were extracted by liquid phase extraction as follows: Sodium chloride was added to the nutrient solution until saturation and organic compounds were extracted with 300 mL of ethyl acetate per 1 L of nutrient solution in a separating funnel. The ethyl acetate phase was filtered through a layer of 2 cm of anhydrous Na_2SO_4 to remove any remaining water. The extraction of the nutrient solution was repeated. The two ethyl acetate extracts were pooled, concentrated *in vacuo* and stored at 4 °C until further analysis. Approximately 100 L of nutrient solution (~root exudates of 400 plants) were pooled to obtain ~3 mg of raw exudate, yielding between 100-200 µg pure compounds after semi-preparative fractionation (next section).

2.2. Root exudate fractionation

For LC-MS analysis and semi-preparative HPLC fractionation, ethyl acetate extracts were dried under a N_2 flow (30°C) and resuspended in H_2O / acetonitrile (1/1, v/v) or H_2O / isopropanol / acetonitrile (1/1/1, v/v/v), respectively. Brachialactone (**1**) was identified based on its molecular mass via LC-MS (Accela HPLC / LTQ Velos MS, Thermo Scientific, Waltham, USA) using a Kinetex 2.6 µm XB-C18 100A reverse phase column (Phenomenex, Torrance, USA) with formate buffer (10 mM, pH 3.7) as polar and acetonitrile as nonpolar eluent (flow rate 0.5 mL min^{-1}).

Selected major compounds and brachialactone (**1**) were subsequently isolated by semi-preparative HPLC (Knauer Smartline, Berlin, Germany), using an EC 250/10 Nucleodur PolarTec 5 µm reverse phase column (Macherey-Nagel, Düren, Germany). Obtained fractions were then analyzed via HRMS (see next section) and those fractions still consisting of several compounds (as also the case for the brachialactone fraction) were subjected to a second purification step on a xSelect HSS Prep T3 5 µm 10 × 150 mm reverse phase column (Waters, Milford, USA). Both fractionation steps were conducted with 0.01 % trifluoroacetic acid as polar and acetonitrile as nonpolar eluent (flow rate 5 mL min^{-1}). The applied eluent gradients are provided in the Tables S1-S3 (supplementary material). Obtained isolates were concentrated by rotary evaporation and subsequently lyophilized to dryness.

2.3. HRMS

High resolution mass-spectra were recorded on a QExactive Plus Electrospray Mass Spectrometer (Thermo Fisher Scientific Waltham, USA) coupled to an Agilent 1290 Ultra Performance Liquid Chromatography System. Measurement parameters were: ESI positive, HESI Source, Capillary Temp 360°C, Sheath gas 60, Aux gas 20, Probe Heater 380°C, Full scan: 100-800 m/z, resolution 35.000, MS2: resolution 17.500, NCE 15, 25, 35. The eluent gradient is provided in Table S4 (supplementary material).

2.4. NMR spectroscopy

NMR-spectra were recorded on an Avance HD III 600MHz spectrometer, equipped with a BBO Prodigy cryo-probe (Bruker, Billerica, USA). Metabolites were dissolved in methanol-d_4 in standard 5 mm NMR tubes or 2 mm MATCH NMR tubes. The ^{1}H and ^{13}C chemical shifts were referenced to the residual solvent signal at $\delta_{H/C}$ 3.35 ppm / 49.0 ppm. HSQC, HMBC, NOESY, COSY and selective 1D-TOCSY spectra were recorded using standard Bruker pulse sequences at 298 K. Selective 2D HMBC (compound 2) was recorded at 279 K in a 2 mm MATCH NMR tube. Due to the low sample amounts obtained (100-200 µg), ^{13}C chemical shifts were indirectly determined by HSQC and HMBC, which were recorded with 2048 points in F2 and 256 increments in F1 and between 40-256 scans (duration 8-44h). For processing and evaluation of NMR spectra, the software SpinWorks 4.2.8.0 (Copyright 2017, K. Marat, University of Manitoba, Canada) was used.

2.5. Computational studies

^{13}C NMR chemical shifts of compounds **1a** (~1 with a C4-O-C19 lactone moiety), **1b** (~1 with a C3-O-C19 lactone moiety) and **2** were calculated according the following procedure: The structures were optimized with the MM2 force field implemented in Chem3D Pro version 13 (2013). Then, the optimized structures were subsequently reoptimized at the PM6 level followed by the RHF/3-21G level and finally by the APDF/6-311++G(2d,p) level of DFT theory within the Gaussian 16 package (2016) . In the final step, the ^{13}C NMR chemical shifts of the reoptimized geometries were computed at the DFT GIAO APDF/Aug-CC-pVTZ //APDF/6-311++G(2d,p) level of theory. TMS as a reference was computed in the same way.

2.6. Assessment of nitrification inhibiting potential

Nitrification inhibiting activity was assessed by means of the *N. europaea* based bioluminescence assay developed by Subbarao et al. (2006) and adjusted by Nuñez et al. (2018).

Briefly, the bioluminescent *N. europaea* IFO 14298 (ATCC 19178) pHLUX20 strain developed by Iizumi et al. (1998) was cultured in a kanamycin (50 µg mL^{-1}) supplemented phosphate buffered growth medium for 6 days at 50 rpm and 28°C. The growth medium was composed of [mM]: KH_2PO_4 5.14, Na_2HPO_4 95.1, $(NH_4)_2SO_4$ 18.91, $NaHCO_3$ 5.95, $CaCl_2$ 0.034, $MgSO_4$ 0.041, Fe (III) EDTA 0.0027. Two hundred mL of liquid culture were centrifuged at 2500 x g for 20 min and the *N. europaea* pellet was resuspended in 50 mL of fresh culture medium. Compounds to be tested were dissolved in 1 µL DMSO, diluted to 100 µL with distilled H_2O and then incubated with 125 µL *N. europaea* culture for 15 min (900 rpm, 15°C) prior to bioluminescence measurements. Bioluminescence was measured on 100 µL aliquots with two technical replicates on a Glomax 20/20 (Promega, Fitchburg, USA) integrating the flash luminescence reaction 2 to 10 s after automated injection of 25 µL of decanal (1 %) in ethanol. Every measurement was repeated with three biological replicates and inhibition was calculated relative to the DMSO blank.

2.7. Statistics

Statistics were performed and plots were created with R version 3.5.3 (R Core Team, 2018) using the packages "lsmeans", "multcompView" and "ggplot2". "lsmeans" package was used to perform an ANOVA and "multcompView" to evaluate statistical significance of nitrification inhibitory effects using Tukey-Tests. Package "ggplot2" was used to create the figures.

3. Results

3.1. Isolation and identification of brachialactone (1) and 3-*epi*-brachialactone (2)

LC-MS analysis of root exudates of *B. humidicola* revealed only one peak (retention time t_r = 11.20 min; Fig. 1) with a molecular mass corresponding to the previously described nitrification inhibitor brachialactone (**1**) (Subbarao et al., 2009), detected as protonated molecular ion with *m/z* 335 $[M+H]^+$. After fractionation of root exudates by semi-preparative HPLC, the fraction

expected to correspond to **1** was evaluated by LC-HRMS and revealed two compounds occurring as double-peak. The two compounds showed maximum UV absorption at 230 nm and molecular masses of *m/z* 335.2217 $[M+H]^+$ and *m/z* 335.2216 $[M+H]^+$, respectively. Separation by subsequent semi-preparative HPLC and evaluation of their 1D and 2D NMR spectra afforded two highly similar chemical structures for **1** and **2** differing only in the configuration at C3. Structure elucidation of the later-eluting fraction and comparison with literature data confirmed brachialactone (**1)** despite C19 was not observable due to very low sample amount. The different stereochemistry at C3, i.e. an interchange of the hydroxyl and the hydroxy-methyl group in **2** compared to **1**, was proven by NOESY correlations of the hydroxymethyl protons 18-H_a (δ 3.51 ppm) and 18-H_b (δ 3.44 ppm) with 1-H_{ax} at δ 0.98 ppm. This assigns the compound as a diastereomer, more precisely as the C3-epimer of **1**, which was defined as 3-*epi*-brachialactone (**2**) (Fig. 2). A $^3J_{CH}$ long range correlation between 4-H at δ 4.56 ppm and C19 at δ 168.00 ppm in the selective HMBC (recorded at 279 K in the 2 mm MATCH NMR tube) of **2** unambiguously established the lactone formed by C4-O-C19 (Fig. S27, supplementary material). Due to the lack of a direct NMR proof for the lactone in compound **1** the ^{13}C chemical shifts of compound **1** with a C4-O-C19 (= **1a**) and with a C3-O-C19 (= **1b**) lactone moiety and for compound **2** were calculated by quantum mechanical DFT calculations at the DFT GIAO APDF/Aug-CC-pVTZ // APDF/6-311++G(2d,p) level of theory (Gaussian 16 package, 2016) and compared with experimental data (Fig. S29 – S31, Table S5, supplementary material). Comparison of the calculated ^{13}C chemical shifts C3 (δ 84.4 ppm) and C4 (δ 82.7 ppm) of **1a** and C3 (δ 93.7 ppm) and C4 (δ 79.9 ppm) of **1b** with the experimental data C3 (δ 82.0 ppm) and C4 (δ 83.7 ppm) strongly suggest a C4-O-C19 lactone moiety in **1**. The NMR-data confirming the chemical structures of **1** and **2** are provided in Tables 1 and 2, respectively. HRMS and NMR spectra are provided in Fig. S1 - S14 (supplementary material).

3.2. Identification of 16-hydroxy-3-*epi*-brachialactone (3) and 3,18-epoxy-9-hydroxy-4,7-*seco*-brachialactone (4)

During NMR analysis of the remaining fractions isolated via semi-preparative fractionation, two additional fractions were identified as brachialactone derivatives (Fig. 3).

The first brachialactone derivative was assigned as 16-hydroxy-3-*epi*-brachialactone (**3**) with a maximum UV absorption at 230 nm and a molecular mass of *m/z* 351.2168 $[M+H]^+$. It has the same C3 stereochemistry as **2**, but carries an additional hydroxyl-group, as indicated by an increase of the molecular mass by Δ16 amu. The C16 position of the hydroxyl-group was deduced by the evaluation of the COSY and HSQC spectra. The methine proton 15-H (δ 1.90 ppm) of the isopropyl moiety at C14 showed a COSY correlation with methyl-group C17 (δ_H 0.89 ppm, *d*, *J*= 6.8 Hz) and showed correlations to the diastereotopic protons of a hydroxymethyl-group (δ_H 3.33 ppm, δ_H 3.43 and δ_C 68.0), which consequently is proposed to be ubicated at position C16. The hydroxylation increases the polarity of the compound, as reflected by the strongly decreased HPLC retention time (t_r = 8.08 min, Fig. 1) compared to the non-hydroxylated brachialactone epimer **2**.

The second brachialactone derivative was elucidated as 3,18-epoxy-9-hydroxy-4,7-*seco*-brachialactone (**4**), possessing UV absorption similar to the previously described compounds (maximum at 230 nm) and a molecular mass of *m/z* 333.2061 $[M+H]^+$. It exhibits a 3,18 epoxide ring (the same C atoms involved in above described isomerism). Additionally, this molecule is characterized by an opening of the lactone ring, which is unique among all other brachialactone forms described so far, and an additional hydroxyl-group at C9. The molecular structure was elucidated based on the COSY, HSQC and HMBC spectra. The relative stereochemistry was deduced by evaluation of the NOESY spectra (as shown in Fig. S28, supplementary material): NOESY correlations between protons 2-H, 5-H, 6-H, 9-H and 20-H indicate axial positions above the molecular plane. The transdiaxial position of proton 1-H_{ax} at δ 0.96 ppm and 2-H at δ 2.83 ppm was indicated by a coupling constant of *J* = 12.4 Hz. NOESY correlations between

protons 1-H_{ax}, 10-H at δ 1.88 ppm and 18-H at δ 2.78 ppm prove positions below the molecular plane and thereby the configuration of the epoxide ring at C3. With a retention time of t_r = 10.60 min (Fig. 1), this molecule is slightly more polar than **1** and **2**, but substantially less polar than **3**. The NMR data confirming the chemical structures of **3** and **4** are provided in Tables 3 and 4, respectively. HRMS and NMR spectra are provided in Fig. S15 – S26 (supplementary material).

3.3. Nitrification inhibitory potential of brachialactone isomers and derivatives

The dose-response curves for the different brachialactone isomers / derivatives tested against *N. europaea* are displayed in Fig. 4. The underlying assay is based on a recombinant, bioluminescent *N. europaea* strain, where bioluminescence as measured parameter correlates with ammonia oxidation, thereby serving as a proxy for the metabolic activity of the test organism. As the tested compounds were solubilized in DMSO prior to addition to the assay medium, the nitrification activities of the treated bacteria are displayed relative to the DMSO-blank. The susceptibility of the applied *N. europaea* batch to DMSO, and the synthetic nitrification inhibitor allylthiourea at effective dosages ED_{50} and ED_{80} (Fig. S32, supplementary material) confirmed the sensitivity of the bioassay (Subbarao et al., 2006; Nuñez el al., 2018). The brachialactone C3-epimer **2** possessed the highest nitrification inhibiting activity (ED_{50} ~ 20 µg mL^{-1} ED_{80} ~ 40 µg mL^{-1}), followed by **4** with intermediate (ED_{50} ~ 40 µg mL^{-1}) and rather low activity for the originally described **1**. Compound **3** did not show any nitrification inhibiting activity in the assessed range of 10-40 µg mL^{-1}. At doses ≥ 20 µg mL^{-1}, NI activities were statistically different (α = 0.05) between all brachialactone isomers / derivatives.

4. Discussion

The structure elucidation of the different brachialactone compounds revealed substantial variability in the stereochemistry at C3. Obviously, the C3 substituents are not only involved in the isomerism between brachialactone (**1**) and the discovered C3-epimers 3-*epi*-

brachialactone (**2**) and 16-hydroxy-3-*epi*-brachialactone (**3**). They are also origin to the epoxide ring described for 3,18-epoxy-9-hydroxy-4,7-*seco*-brachialactone (**4**). This fundamental finding is corroborated by previous reports on stereoisomerism and epoxide rings at fusicoccane-associated C3 atoms (Ballio et al., 1991; Muromtsev et al., 1994; Sassa et al., 2002). It is founded in the common precursors of plant fusicoccanes, which has been – in analogy to fungi (Kato et al., 1998; Kato et al., 1999) – proposed to be (+)-fusicocca-2,10(14)-diene (Sassa et al., 1999). This molecule is planar at the C3 atom (double bond), allowing the synthesis of different stereoisomers upon conversion of the C3 atom into a stereo center by hydrogenation or hydroxylation. The respective biosynthetic pathway has been proposed by Sassa et al. (2002).

The brachialactone isomers and derivatives discovered in our study revealed, except **3**, a significantly higher NI activity than **1**, the brachialactone form originally described by Subbarao et al. (2009). The fact that both brachialactone isomers **1** and **2** co-eluted in HPLC separations, clearly suggested that the initial description of **1** as potent nitrification inhibitor was based on a mixture of both isomers and unconsciously on the activity of **2**.

The discrepancy of NI activity of both isomers was further corroborated by earlier reports highlighting the significance of the above discussed stereochemistry for receptor binding and associated varying biological activity of fusicoccanes (Ballio et al., 1991; Sassa et al., 2002). In congruence to our study, Sassa et al. (2002) evaluated the germination stimulating activity of fusicoccine (FC) A and different precursors and isomers, namely FC H and FC Q, and their C3-epimers 3-*epi*-FC H and 3-*epi*-FC Q. They confirmed that specifically C3-epimers, whose configurations at C3 correspond to that of **2**, were biologically active, while FC-H and FC-Q, corresponding to the molecule structure of **1**, did not reveal any activity. The coherence of our results suggests that the biological activity of **2** is founded in its fusicoccane core structure, a conclusion that is supported by the observed biological activity of **4**, which does not possess a lactone ring, but the same fusicoccane core structure.

5. Conclusions and Outlook

Here we report on the discovery of three so far undescribed brachialactone isomers and derivatives. Assessment of their nitrification inhibiting activity revealed 3-*epi*-brachialactone (**2**) rather than the previously described brachialactone (**1)** to be the main bioactive, nitrification inhibiting compound produced by *B. humidicola*. The remarkable analogy of encountered biological activities of these brachialactone C3-epimers with previous reports on the activity of fusicoccin (FC) derivatives (Ballio et al., 1991; Sassa et al., 2002) strongly suggests that the nitrification inhibition activity of brachialactones is predicated on their FC nature. The structural and pharmacological proximity between brachialactone and FC, together with the fact that the biological activity of different fusicoccanes (compounds sharing the same core 5-8-5 ring structure) is proposed to be founded in a common molecular mechanism, suggests similar modes of action. With respect to the inhibitory effect upon nitrifying microorganisms, this hypothetical conclusion is still difficult to align with the current understanding of FC interference with 14-3-3 regulatory proteins (de Boer, 1997), which have exclusively been assigned to eukaryotes, but not to prokaryotes (Ferl et al., 2002). On the other hand, our results suggest that brachialactones may have another, so far undiscovered regulatory function in plants. The genetic and physiological evidence for this speculation is yet to be given, emphasizing that fusicoccanes have been described as a new class of phytohormones (Muromtsev, 1994). These hypotheses should be taken into account upon future studies, integrating metabolomics and genomics of both *B. humidicola* and affected nitrifying soil microorganisms to further unravel the yet poorly understood modes of action of these newly discovered plant derived bioactive compounds.

6. Contributions

KE conducted the presented study, wrote the manuscript and modified it according to suggestions and corrections of the co-authors. JS and CB guided the isolation and purification of brachialactone isomers and derivatives. JS performed LC-MS measurements. CB and JC recorded NMR spectra and elucidated the chemical structures. UB gave advise during the isolation of brachialactone isomers and facilitated KE access to his lab facilities. FW provided access to and supported LC-MS analysis. JN guided the performance of the bioassays, JA was the leading scientist at CIAT and enabled KE access to his lab facilities. HK contributed to the study design and data interpretation. GN and GC co-supervised the study. FR was leading senior scientist of the study. All authors contributed to manuscript revision, read, and approved the submitted version.

7. Acknowledgements

The authors would like to thank Mr. Sebastian Mira and Mrs. Supriya Verma for their assistance during hydroponic cultivation of *B. humidicola* and root exudate collection. We are grateful to Mrs. Nadia Jimenez for conducting preliminary screenings for bioactive compounds. For their support during the bioassays, we are thankful to Mrs. Ashly Arevalo and Mr. Daniel Villegas. We thank Mr. Mario Wolf for his support during NMR analysis and Mrs. Iris Klaiber for her advice during LC-MS analysis and interpretation. In addition, the authors acknowledge Dr. Guntur Subbarao for providing the *N. europaea* bioassay to CIAT and for the valuable discussions.

Funding: The first author (K. Egenolf) is grateful to the "Water-People-Agriculture" Research Training Group funded by the Anton & Petra Ehrmann-Foundation for financing this study as part of his doctoral research. Furthermore, we thank the German Ministry of Education and Research (BMBF) and Colciencias for funding the project "Eco-efficient management of tropical savannas (ECOMASA)" (grant no. 01DN18031), which enabled the research visit of K. Egenolf at CIAT. This study was further co-funded by CIAT within the "LivestockPlus"

project under the CGIAR Research Program (CRP) on Climate Change, Agriculture and Food Security (CCAFS) and the Livestock CRP.

Declaration of interest: none.

Fig. 1. HPLC-PDA chromatogram of the extracted root exudates of *Brachiaria humidicola* with peaks corresponding to brachialactone isomers and derivatives, including retention time (t_r).

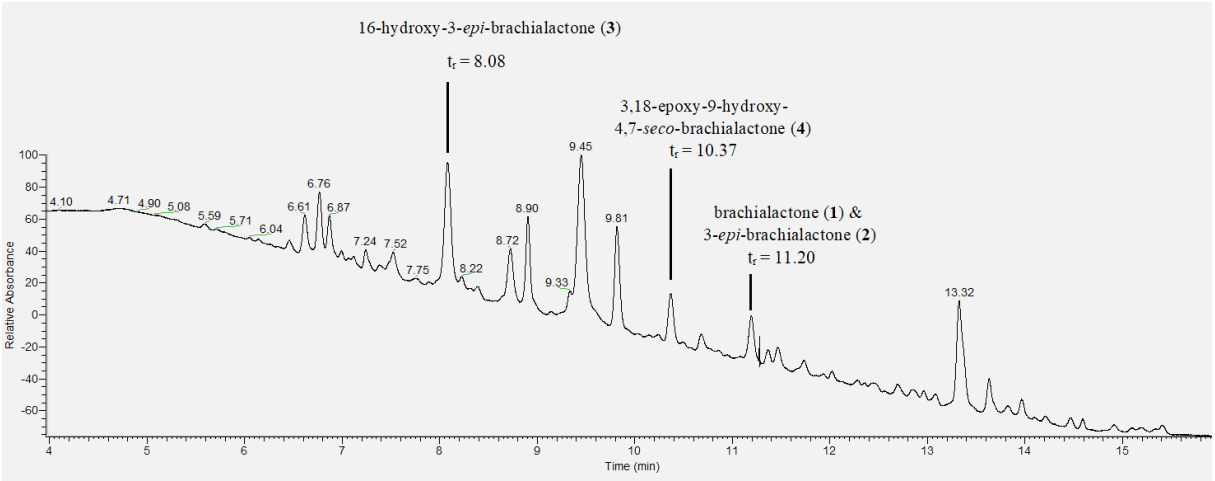

Fig. 2. Chemical structures of brachialactone (**1**) and 3-*epi*-brachialactone (**2**) isolated from the root exudates of *Brachiaria humidicola*. Both isomers differ in their absolute configuration at C3.

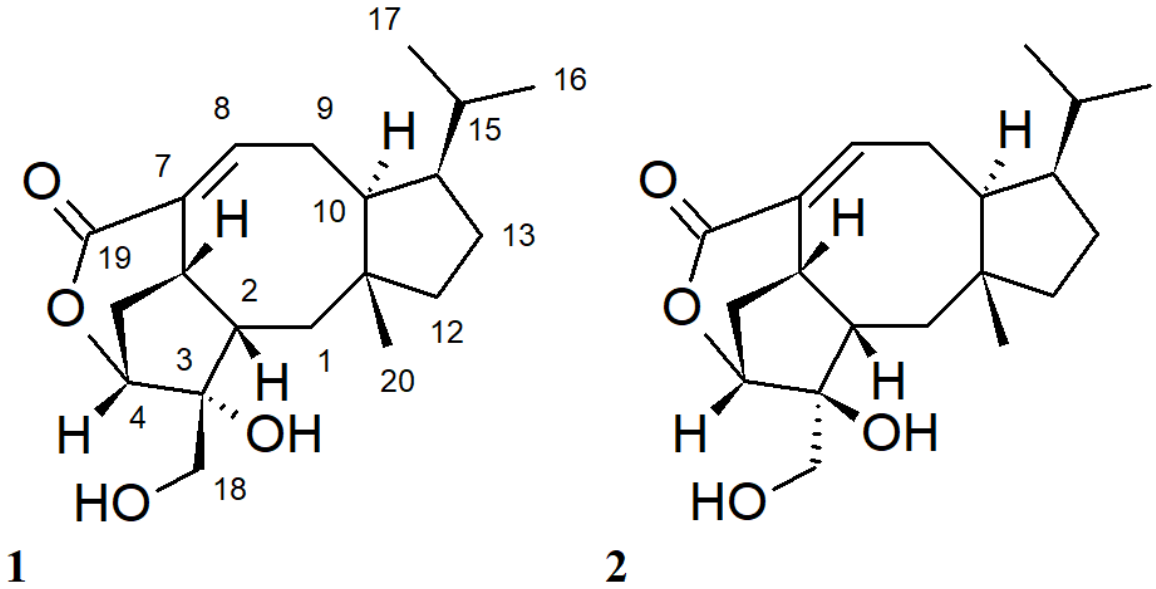

Fig. 3. Chemical structures of the brachialactone derivatives 16-hydroxy-3-*epi*-brachialactone (**3**) and 3,18-epoxy-9-hydroxy-4,7-*seco*-brachialactone (**4**) isolated from the root exudates of *Brachiaria humidicola.*

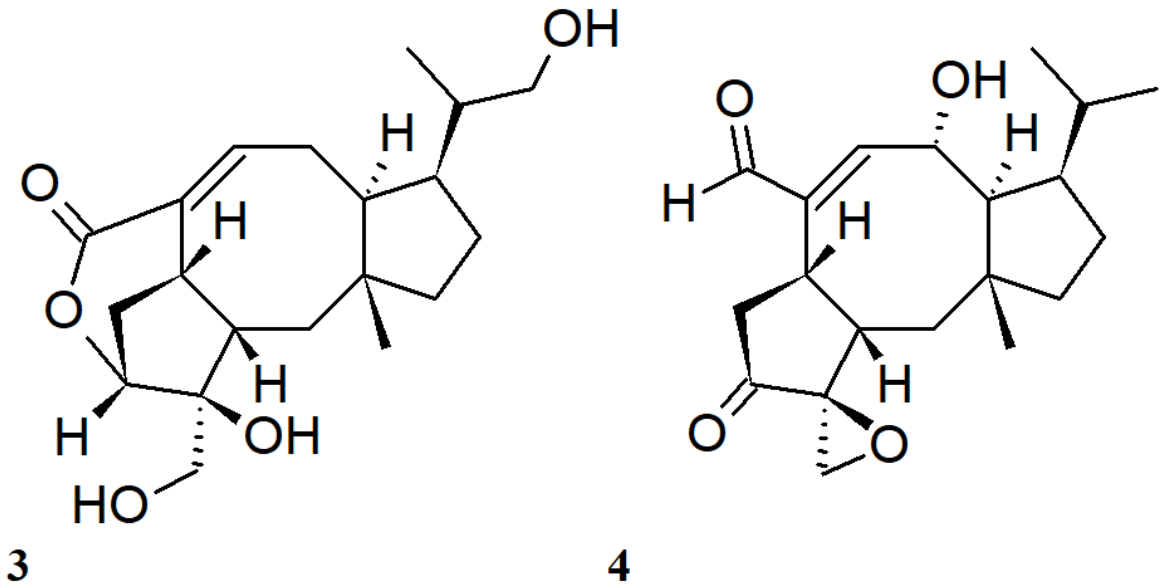

3 **4**

Fig. 4. Relative metabolic activity (determined via bioluminescence measurements) of *Nitrosomonas europaea* IFO 14298 (ATCC 19178) pHLUX20 cultures in dependence of tested doses (10 – 40 µg mL^{-1}) of different brachialactone isomers / derivatives. All brachialactone compounds were solubilized in DMSO and spiked to the assay medium. Results are displayed relative to a DMSO blank. Data represent the mean of three technical replications. Error bars represent standard error (SE). At doses ≥ 20 µg mL^{-1}, relative metabolic activities were statistically different ($\alpha = 0.05$) between all brachialactone isomers / derivatives.

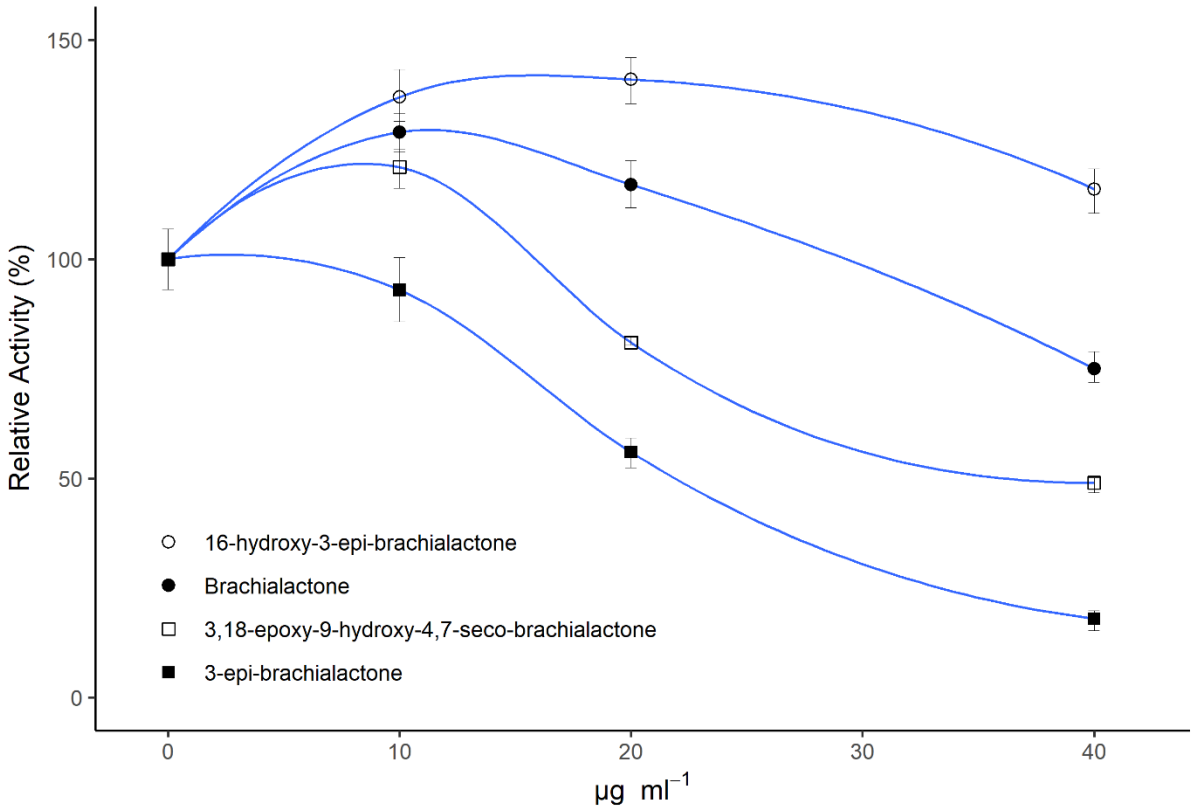

Table 1. NMR-spectral analysis of brachialactone (**1**) in MeOH-d_4.

Atom	δH (ppm), multiplicity, *J* (Hz)	δC (ppm)	HMBC	NOESY
1ax	1.39 dd (12.1, 14.5)	37.9		
1eq	1.54 dd (5.4, 14.7)	-		
2	2.04 ddd (5.4, 5.4, 12.5)	47.5	C7	18a, 20
3	-	82.0		
4	4.58 q-like (1.9)	83.7		5, 18a
5	1.97-1.95 m	33.4	C2, C7	4, 6
6	3.35 ov	40.1		5, 20
7	-	131.1		
8	7.16 brt (8.7)	145.8		10
9a	2.44 brdd (7.8, 12.9)	24.7		
9b	2.34 ddd (8.7, 12.2, 12.2)	-		20
10	1.67 ov	55.6		8, 14
11	-	44.5		
12a	1.46 dt (7.8, 12.1, 12.1)	44.8		
12b	1.42 ov	-		
13a	1.66 ov	24.0		
13b	1.57 ov	-		20
14	2.28-2.22 m	48.7		10
15	1.96-1.91 m	29.8		
16	0.97 d (6.7)	23.6		
17	0.89 d (6.7)	20.0		
18a	3.44 d (11.2)	68.1		2, 4
18b	3.39 d (11.2)	-		
19	-	n.o.		
20	1.04 s	18.2	C1, C10, C11, C12	2, 6, 9a, 13b

Coupling constants were directly taken form the NMR spectrum and were not averaged.

Abbreviations: s = singlet, d = doublet, dd = double doublet, ddd = triple doublet, t = triplet, dt = double triplet, q = quartet, m = multiplet, br = broad, ax = axial, eq = equatorial, ov = overlapped with other signal, n.o. = not observable.

Table 2. NMR-spectral analysis of 3-*epi*-brachialactone (**2**) in MeOH-d_4.

Atom	δH (ppm), multiplicity, *J* (Hz)	δC (ppm)	HMBC	NOESY
1ax	0.98 dd (13.6, 13.6)	37.4		10, 18a, 18b
1eq	1.83 dd (5.3, 14.0)	-		2, 20
2	2.31 ddd (5.7, 5.7, 12.6)	53.4		1eq, 6, 20
3	-	84.0		
4	4.56 m	86.4	C19	5a
5a	2.25 d-like (3.5, 3.5, 12.7)	32.1		4, 6
5b	1.92 brd			
6	3.45 brm	40.4		2, 5a, 9b, 20
7	-	128.1		
8	7.17 t-like (8.4)	146.9	C7, C19	9a
9a	2.43 ddd (0.7, 7.9, 12.7)	24.9		8
9b	2.34 ddd (8.9, 12.1, 12.1)	-		6, 17
10	1.62 dd (11.6, 11.6)	55.6		1ax
11	-	44.9		
12	1.42 m	44.5		20
13a	1.66 ov	24.4		
13b	1.53 ov	-		17, 20
14	2.24 m	48.7		
15	1.96-1.87, 1.93 m	29.9		
16	0.96 d (6.5)	23.8		
17	0.89 d (6.8)	20.1		9b, 13b, 20
18a	3.51 d (11.4)	64.1		1ax
18b	3.44 brd (11.3)	-		1ax
19	-	168.0		
20	1.03 s	18.0		1eq, 2, 6, 12, 13b, 17

Coupling constants were directly taken form the NMR spectrum and were not averaged.

Abbreviations: s = singlet, d = doublet, dd = double doublet, ddd = triple doublet, t = triplet, dt = double triplet, q = quartet, m = multiplet, br = broad, ax = axial, eq = equatorial, ov = overlapped with other signal, n.o. = not observable.

Table 3. NMR-spectral analysis of 16-hydroxy-3-*epi*-brachialactone (**3**) in MeOH-d_4.

Atom	δH (ppm), multiplicity, J (Hz)	δC (ppm)	HMBC	NOESY
1ax	1.00 dd (13.5, 13.5)	37.5		10, 18a
1eq	1.86 dd (4.9, 14.0)	-		
2	2.32 ddd (5.0, 5.0, 13.1)	53.2		20
3	-	84.1		
4	4.56 brt (2.7)	86.1		5a, 5b
5a	2.25 ddd (3.5, 3.5, 13.1)	32.0		4
5b	1.93 brd (13.0)	-	C2, C3, C7	4
6	3.45 brm	40.2		20
7	-	131.2		
8	7.18 dd (8.5)	146.6	C19	9, 10
9a	2.39-2.33 m	24.4		8
9b	2.39-2.33 m	-		8
10	1.67 ddd (3.5, 9.2, 12.7)	55.2		1ax, 8, 14
11	-	44.4		
12a	1.49-1.43 m	44.4		
12b	1.44-1.39 m	-		
13a	1.69-1.64 m	23.3		
13b	1.60-1.55 m	-		
14	2.53-2.46 m	42.6		10
15	1.92-1.87 m	37.1		16, 17
16a	3.33 dd (7.4, 10.5)	68.0		15
16b	3.43 dd (6.4, 10.4)	-		15
17	0.89 d (6.8)	14.3		15, 20
18a	3.52 d (11.7)	63.9		1ax
18b	3.44 d (11.4)	-		
19	-	166.4		
20	1.04 s	17.8	C1, C10, C11, C12	1eq, 2, 6, 17

Coupling constants were directly taken form the NMR spectrum and were not averaged.

Abbreviations: s = singlet, d = doublet, dd = double doublet, ddd = triple doublet, t = triplet, dt = double triplet, q = quartet, m = multiplet, br = broad, ax = axial, eq = equatorial, ov = overlapped with other signal, n.o. = not observable.

Table 4. NMR-spectral analysis of 3,18-epoxy-9-hydroxy-4,7-*seco*-brachialactone (**4**) in MeOH-d_4.

Atom	δH (ppm), multiplicity, *J* (Hz)	δC (ppm)	HMBC	NOESY
1ax	0.96 dd (12.3, 14.2)	37.4		8, 18
1eq	1.35 dd (3.8, 14.3)	-		2, 18, 20
2	2.83 ddd (3.7, 8.0, 12.4)	40.4		1eq, 6
3	-	62.4		
4	-	212.0		
5a	2.70 bd (18.6)	39.6	C2, C4	6, 19
5b	2.62 dd (8.6, 18.6)	-		6
6	3.59 brt (8.5)	33.9	C2, C3, C4, C19	2, 5a, 5b, 9, 20
7	-	137.7		
8	6.74 brd (6.4)	166.6	C6, C19	1ax, 10, 19
9	4.93 dd (6.4, 11.8)	68.7		6, 17, 20
10	1.88 dd (9.9, 11.0)	60.4	C8, C9	8, 14
11	-	42.7		
12a	1.51 brdd (9.2, 12.2)	45.0		
12b	1.46 brddd (2.2, 8.0, 12.2)	-		
13a	1.73-1.67 m	24.4		
13b	1.64-1.56 m	-		
14	2.52 m	48.8		10
15	2.61 ov	30.5		
16	0.99 d (6.9)	21.3	C14, C15	20
17	1.01 d (6.9)	23.2	C14, C15	9
18a	2.78 d (6.1)	52.1	C2, C3, C4	1ax, 1eq
18b	2.78 d (6.1)	-	C2, C3, C4	1ax, 1eq
19	9.35 d (1.3)	196.6	C6, C7	5a, 8
20	1.15 s	19.4	C1, C10, C11, C12	1eq, 6, 9, 16

Coupling constants were directly taken form the NMR spectrum and were not averaged.

Abbreviations: s = singlet, d = doublet, dd = double doublet, ddd = triple doublet, t = triplet, dt = double triplet, q = quartet, m = multiplet, br = broad, ax = axial, eq = equatorial, ov = overlapped with other signal, n.o. = not observable

References

Arp, D.J., Stein, L.Y., 2003. Metabolism of inorganic N compounds by ammonia-oxidizing bacteria. Critical reviews in biochemistry and molecular biology 38 (6), 471–495. https://doi.org/10.1080/10409230390267446.

Ballio, A., Castellano, S., Cerrini, S., Evidente, A., Randazzo, G., Segre, A.L., 1991. 1H NMR conformational study of fusicoccin and related compounds: molecular conformation and biological activity. Phytochemistry 30 (1), 137–146. https://doi.org/10.1016/0031-9422(91)84114-8.

Bardgett, R.D., McAlister, E., 1999. The measurement of soil fungal:bacterial biomass ratios as an indicator of ecosystem self-regulation in temperate meadow grasslands. Biol Fert Soils 29 (3), 282–290. https://doi.org/10.1007/s003740050554

Boer, A.H. de, Vries-van Leeuwen, I.J. de, 2012. Fusicoccanes: diterpenes with surprising biological functions. Trends in plant science 17 (6), 360–368. https://doi.org/10.1016/j.tplants.2012.02.007.

Boer, B. de, 1997. Fusicoccin — a key to multiple 14-3-3 locks? Trends in plant science 2 (2), 60–66. https://doi.org/10.1016/S1360-1385(97)82564-2.

Byrnes, R.C., Nuñez, J., Arenas, L., Rao, I., Trujillo, C., Alvarez, C., Arango, J., Rasche, F., Chirinda, N., 2017. Biological nitrification inhibition by Brachiaria grasses mitigates soil nitrous oxide emissions from bovine urine patches. Soil Biology and Biochemistry 107, 156–163. https://doi.org/10.1016/j.soilbio.2016.12.029.

Chem3D Pro, version 13, Cambridge Soft, Cambridge MA, USA, 2013.

Clint, G.M., Blatt, M.R., 1989. Mechanisms of fusicoccin action: evidence for concerted modulations of secondary K^+ transport in a higher plant cell. Planta 178 (4), 495–508. https://doi.org/10.1007/BF00963820.

Coskun, D., Britto, D.T., Shi, W., Kronzucker, H.J., 2017. Nitrogen transformations in modern agriculture and the role of biological nitrification inhibition. Nature plants 3, 17074. https://doi.org/10.1038/nplants.2017.74.

Felle, H., Brummer, B., Bertl, A., Parish, R.W., 1986. Indole-3-acetic acid and fusicoccin cause cytosolic acidification of corn coleoptile cells. Proceedings of the National Academy of Sciences of the United States of America 83 (23), 8992–8995. https://doi.org/10.1073/pnas.83.23.8992.

Ferl, R.J., Manak, M.S., Reyes, M.F., 2002. The 14-3-3s. Genome biology 3 (7), reviews3010. https://doi.org/10.1186/gb-2002-3-7-reviews3010.

Gaussian 16, Revision A.03: Frisch, M. J., Trucks, G. W., Schlegel, H. B., Scuseria, G. E., Robb, M. A., Cheeseman, J. R., Scalmani, G., Barone, V., Petersson, G. A., Nakatsuji, H., Li, X., Caricato, M., Marenich, A. V., Bloino, J., Janesko, B. G., Gomperts, R., Mennucci, B., Hratchian, H. P., Ortiz, J. V., Izmaylov, A. F., Sonnenberg, J. L., Williams-Young, D., Ding, F., Lipparini, F., Egidi, F., Goings, J., Peng, B., Petrone, A., Henderson, T., Ranasinghe, D., Zakrzewski, V. G., Gao, J., Rega, N., Zheng, G., Liang, W., Hada, M., Ehara, M., Toyota, K., Fukuda, R., Hasegawa, J., Ishida, M., Nakajima, T., Honda, Y., Kitao, O., Nakai, H., Vreven, T., Throssell, K., Montgomery, J. A., Jr., Peralta, J. E., Ogliaro, F., Bearpark, M. J., Heyd, J. J., Brothers, E. N., Kudin, K. N., Staroverov, V. N., Keith, T. A., Kobayashi, R., Normand, J., Raghavachari, K., Rendell, A. P., Burant, J. C., Iyengar, S. S., Tomasi, J., Cossi, M., Millam, J. M., Klene, M., Adamo, C., Cammi, R., Ochterski, J. W., Martin, R. L., Morokuma, K., Farkas, O., Foresman, J. B., Fox, D. J. Gaussian, Inc., Wallingford CT, 2016.

Gopalakrishnan, S., Subbarao, G.V., Nakahara, K., Yoshihashi, T., Ito, O., Maeda, I., Ono, H., Yoshida, M., 2007. Nitrification Inhibitors from the root tissues of Brachiaria humidicola, a tropical grass. Journal of agricultural and food chemistry 55 (4), 1385–1388. https://doi.org/10.1021/jf062593o.

475 Hooper, A.B., Vannelli, T., Bergmann, D.J., Arciero, D.M., 1997. Enzymology of the
476 oxidation of ammonia to nitrite by bacteria. Antonie van Leeuwenhoek 71 (1), 59–67.
477 https://doi.org/10.1023/A:1000133919203.
478 Iizumi, T., Mizumoto, M., Nakamura, K., 1998. A Bioluminescence Assay Using
479 Nitrosomonas europaea for Rapid and Sensitive Detection of Nitrification Inhibitors.
480 Applied and Environmental Microbiology 64 (10), 3656–3662.
481 Karwat, H., Egenolf, K., Nuñez, J., Rao, I., Rasche, F., Arango, J., Moreta, D., Arevalo, A.,
482 Cadisch, G., 2018. Low ^{15}N Natural Abundance in Shoot Tissue of Brachiaria humidicola
483 Is an Indicator of Reduced N Losses Due to Biological Nitrification Inhibition (BNI).
484 Frontiers in Microbiology 9:2383. https://doi.org/10.3389/fmicb.2018.02383.
485 Kato, N., Zhang, C.-S., Matsui, T., Iwabuchi, H., Mori, A., Ballio, A., Sassa, T., 1998.
486 Isolation of (+)-fusicocca-2,10(14)-diene, a 5-8-5 tricyclic diterpene hydrocarbon
487 biosynthetically related to the fusicoccin aglycon from Fusicoccum amygdali and
488 confirmation of its structure by total synthesis. J. Chem. Soc., Perkin Trans. 1 (16), 2473–
489 2474. https://doi.org/10.1039/a805033c.
490 Kato, N., Zhang, C.-S., Mori, A., Tajima, N., Sassa, T., Graniti, A., 1999. Transformation of
491 fusicocca-2,10(14)-dien-8β-ol into fusicoccin J by the fusicoccin-producing fungus,
492 Phomopsis (Fusicoccum) amygdali. Support for the intermediacy of fusicocca-2,10(14)-
493 diene in the fusicoccin biosynthesis. Chem. Commun. (4), 367–368.
494 https://doi.org/10.1039/a809496i.
495 Lata, J.C., Degrange, V., Raynaud, X., Maron, P.A., Lensi, R., Abbadie, L., 2004. Grass
496 populations control nitrification in savanna soils. Funct Ecology 18 (4), 605–611.
497 https://doi.org/10.1111/j.0269-8463.2004.00880.x.
498 Lodhi, M.A.K., Killingbeck, K.T., 1980. Allelopathic inhibition of nitrification and nitrifying
499 bacteria in a ponderosa pine (Pinus ponderosa Dougl.) community. American Journal of
500 Botany 67 (10), 1423–1429. https://doi.org/10.1002/j.1537-2197.1980.tb07777.x.

Moorhead, G., Douglas, P., Morrice, N., Scarabel, M., Aitken, A., MacKintosh, C., 1996. Phosphorylated nitrate reductase from spinach leaves is inhibited by 14-3-3 proteins and activated by fusicoccin. Current Biology 6 (9), 1104–1113. https://doi.org/10.1016/S0960-9822(02)70677-5.

Muromtsev, G.S., Voblikova, V.D., Kobrina, N.S., Koreneva, V.M., Krasnopolskaya, L.M., Sadovskaya, V.L., 1994. Occurrence of fusicoccanes in plants and fungi. J Plant Growth Regul 13 (1), 39–49. https://doi.org/10.1007/BF00210706.

Nuñez, J., Arevalo, A., Karwat, H., Egenolf, K., Miles, J., Chirinda, N., Cadisch, G., Rasche, F., Rao, I., Subbarao, G., Arango, J., 2018. Biological nitrification inhibition activity in a soil-grown biparental population of the forage grass Brachiaria humidicola. Plant Soil 426 (1-2), 401–411. https://doi.org/10.1007/s11104-018-3626-5.

R Core Team, 2018. R: A language and environment for statistical computing. https://www.R-project.org.

Rice, E.L., Pancholy, S.K., 1972. Inhibition of nitrification by climax ecosystems. American Journal of Botany 59 (10), 1033–1040. https://doi.org/10.1002/j.1537-2197.1972.tb10183.x.

Robertson, G.P., Vitousek, P.M., 1981. Nitrification Potentials in Primary and Secondary Succession. Ecology 62 (2), 376–386. https://doi.org/10.2307/1936712.

Sassa, T., Tajima, N., Sato, M., Takahashi, A., Kato, N., 2002. Fusicoccins P and Q, and 3-epifusicoccins H and Q, new polar fusicoccins from isolate Niigata 2-A of a peach Fusicoccum canker fungus. Bioscience, biotechnology, and biochemistry 66 (11), 2356–2361. https://doi.org/10.1271/bbb.66.2356.

Sassa, T., Zhang, C.S., Tajima, N., Kato, N., 1999. 16-O-Demethyl Fusicoccin J and Its 3-Epimer from Fusicoccum amygdali, and Their Seed Germination-stimulating Activity in the Presence of Abscisic Acid. Bioscience, biotechnology, and biochemistry 63 (5), 951–954. https://doi.org/10.1271/bbb.63.951.

527 Stark, J.M., Hart, S.C., 1997. High rates of nitrification and nitrate turnover in undisturbed
528 coniferous forests. Nature 385, 61-64. https://doi.org/10.1038/385061a0.
529 Subbarao, G.V., Ishikawa, T., Ito, O., Nakahara, K., Wang, H.Y., Berry, W.L., 2006. A
530 bioluminescence assay to detect nitrification inhibitors released from plant roots: a case
531 study with Brachiaria humidicola. Plant Soil 288 (1), 101–112.
532 https://doi.org/10.1007/s11104-006-9094-3.
533 Subbarao, G.V., Nakahara, K., Hurtado, M.P., Ono, H., Moreta, D.E., Salcedo, A.F.,
534 Yoshihashi, A.T., Ishikawa, T., Ishitani, M., Ohnishi-Kameyama, M., Yoshida, M.,
535 Rondon, M., Rao, I.M., Lascano, C.E., Berry, W.L., Ito, O., 2009. Evidence for biological
536 nitrification inhibition in Brachiaria pastures. Proceedings of the National Academy of
537 Sciences of the United States of America 106 (41), 17302–17307.
538 https://doi.org/10.1073/pnas.0903694106.
539 Subbarao, G.V., Nakahara, K., Ishikawa, T., Yoshihashi, T., Ito, O., Ono, H., Ohnishi-
540 Kameyama, M., Yoshida, M., Kawano, N., Berry, W.L., 2008. Free fatty acids from the
541 pasture grass Brachiaria humidicola and one of their methyl esters as inhibitors of
542 nitrification. Plant Soil 313 (1-2), 89–99. https://doi.org/10.1007/s11104-008-9682-5.
543 Sylvester-Bradley, R., Mosquera, D., Méndez, J.E., 1988. Inhibition of nitrate accumulation
544 in tropical grassland soils: effect of nitrogen fertilization and soil disturbance. Journal of
545 Soil Science 39 (3), 407–416. https://doi.org/10.1111/j.1365-2389.1988.tb01226.x.
546 Theron, J.J., 1951. The influence of plants on the mineralization of nitrogen and the
547 maintenance of organic matter in the soil. J. Agric. Sci. 41 (04), 289.
548 https://doi.org/10.1017/S0021859600049467.
549

Supplementary Material

Brachialactone isomers and derivatives of *Brachiaria humidicola* reveal contrasting nitrification inhibiting activity

Konrad Egenolf[a,d], Jürgen Conrad[b], Jochen Schöne[c], Christina Braunberger[b], Uwe Beifuß[b], Frank Walker[c], Jonathan Nuñez[d,1], Jacobo Arango[d], Hannes Karwat[a,d,2], Georg Cadisch[a], Günter Neumann[e], Frank Rasche[a*]

[a]Institute of Agricultural Sciences in the Tropics (Hans-Ruthenberg-Institute), University of Hohenheim, 70593 Stuttgart, Germany

[b]Institute of Chemistry, University of Hohenheim, 70593 Stuttgart, Germany

[c]Institute of Phytomedicine, University of Hohenheim, 70593 Stuttgart, Germany

[d]The Alliance of Bioversity International and the International Center for Tropical Agriculture (CIAT), Km 17 Recta Cali-Palmira, A.A. 6713, Cali, Colombia

[e]Institute of Crop Sciences, University of Hohenheim, 70593 Stuttgart, Germany

[1]Present address: Manaaki Whenua – Landcare Research, PO Box 69040, Lincoln 7640, New Zealand

[2]Present address: Centro Internacional de Mejoramiento de Maíz y Trigo (CIMMYT), Km 45 Carretera México-Veracruz, Col. El Batán, Texcoco, Edo. de Mexico 56130, Mexico

***Corresponding author:**

Dr. Frank Rasche

Phone: +49 (0) 711 459 24137

Fax: +49 (0) 711 459 22304

Email: frank.rasche@uni-hohenheim.de

Table S1. Gradient analytical LC-MS. Column: Phenomenex Kinetex 2.6µ XB-C18 100A, flow rate: 0.5 mL min^{-1}.

Time (min)	% nonpolar eluent (acetonitrile)	% polar eluent (10mM formate buffer)
0.00	15	85
1.00	15	85
11.00	100	0
13.00	100	0
13.10	15	85
16.00	15	85

Table S2. Gradient 1. semi-preparative HPLC separation. Column: *Macherey-Nagel EC 250/10 Nucleodur PolarTec 5µm*, flow rate: 5.0 mL min^{-1}.

Time (min)	% nonpolar eluent (acetonitrile)	% polar eluent (0.01% TFA)
0.00	15	85
2.00	15	85
56.00	55	45
92.00	100	0
98.00	100	0
100.00	15	85

589 **Table S3.** Gradient 2. semi-preparative HPLC separation. Column: *Waters xSelect HSS Prep*

590 *T3 5µm 10x150mm*, flow rate 5.0 mL min^{-1}.

Time (min)	% nonpolar eluent (100% acetonitrile)	% polar eluent (0.01% TFA)
0.00	40	60
3.00	40	60
21.00	45	55
24.00	100	0
28.00	100	0
30.00	40	60

591

592

593 **Table S4.** Gradient UPLC-MS for 3-*epi*-brachialactone quantification. Column: *Waters*

594 *AQUITY UPLC HSS 1.8µm 2.1x150mm*, 40°C, flow rate 0.35 mL min^{-1}.

Time (min)	% nonpolar eluent (acetonitrile, 0.2% formic acid)	% polar eluent (0.01% Formic Acid)
0.00	20	80
5.00	25	75
20.00	60	40
30.00	95	5
35.00	95	5
36.00	20	80
39.00	20	80

595

596

597

Fig S1. HRMS-spectrum of brachialactone

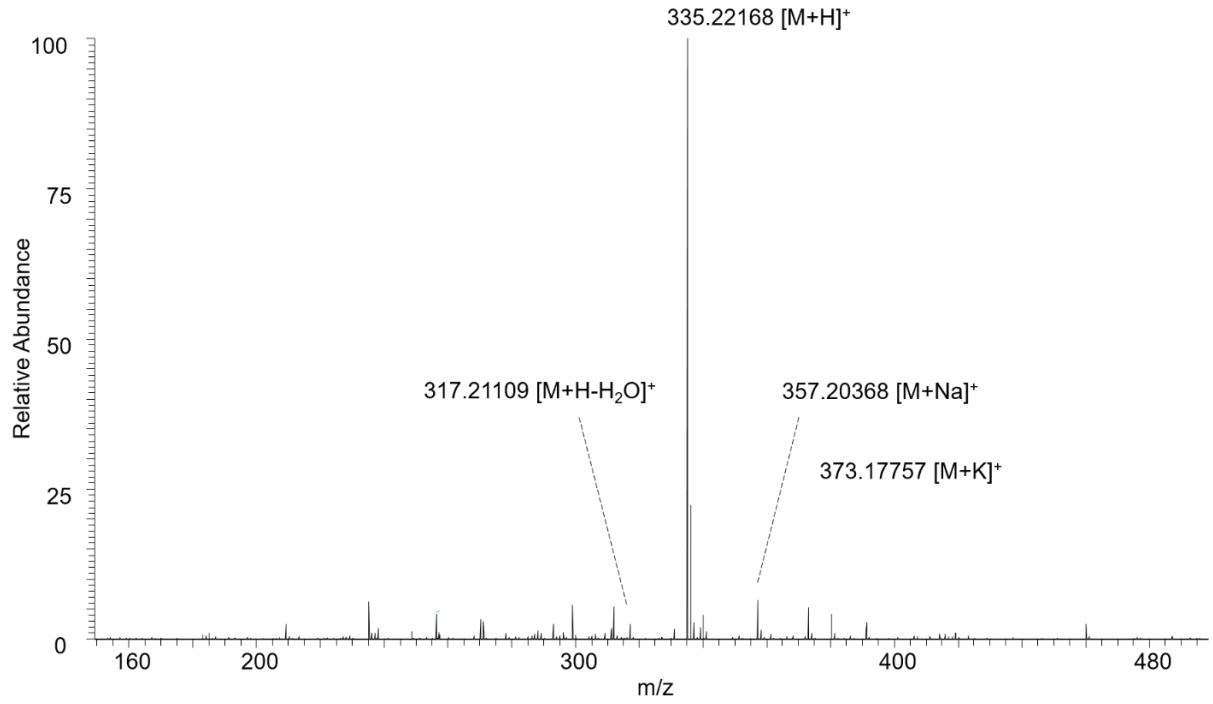

Fig S2. ^{1}H NMR spectrum of brachialactone in MeOH-*d4* at 600 MHz.

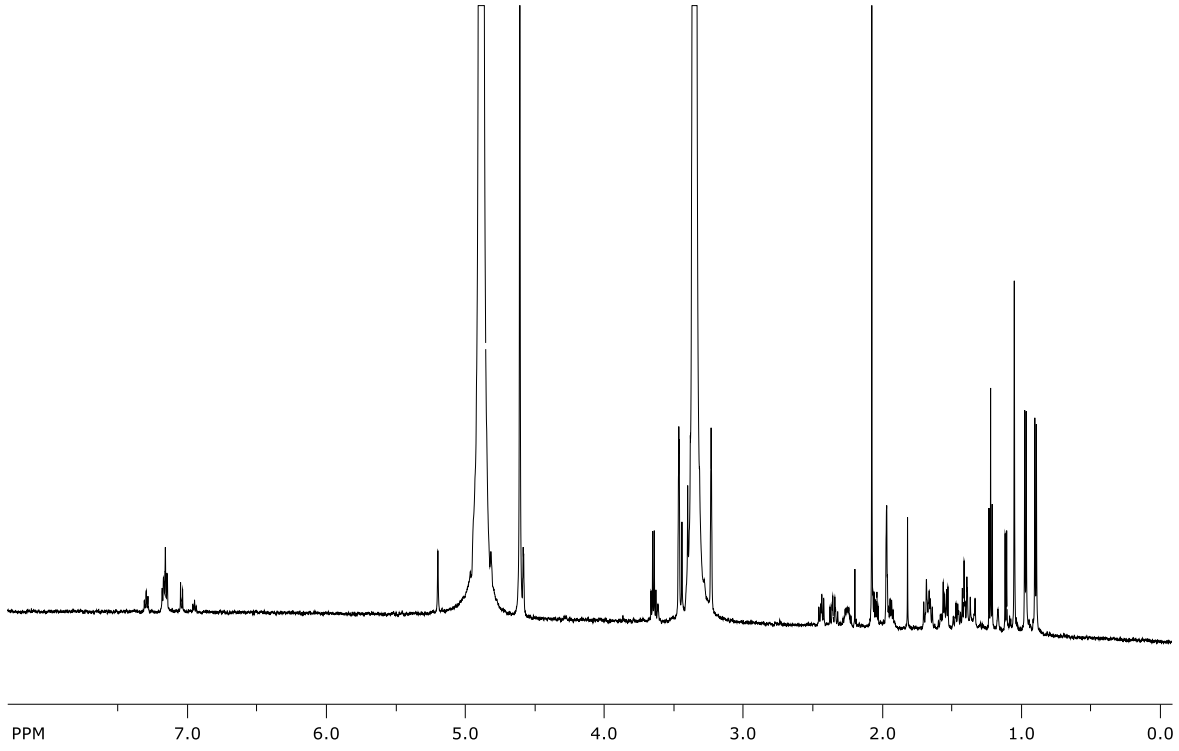

Fig S3. COSY spectrum of brachialactone in MeOH-*d4* at 600 MHz.

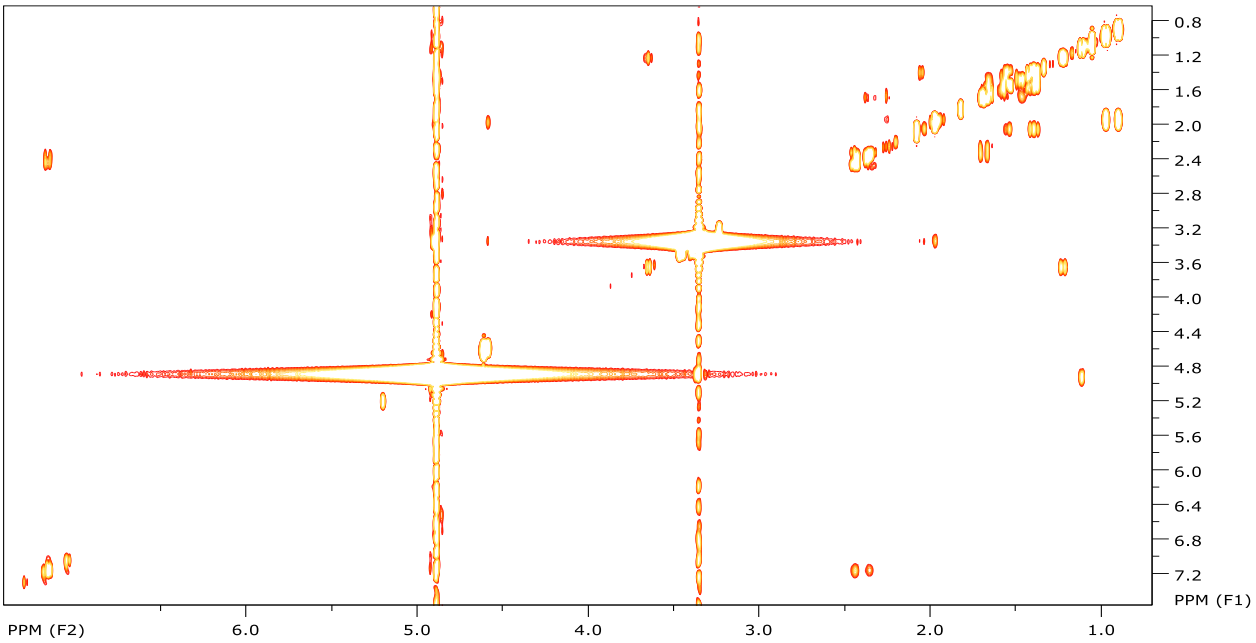

Fig S4. NOESY spectrum of brachialactone in MeOH-*d4* at 600 MHz.

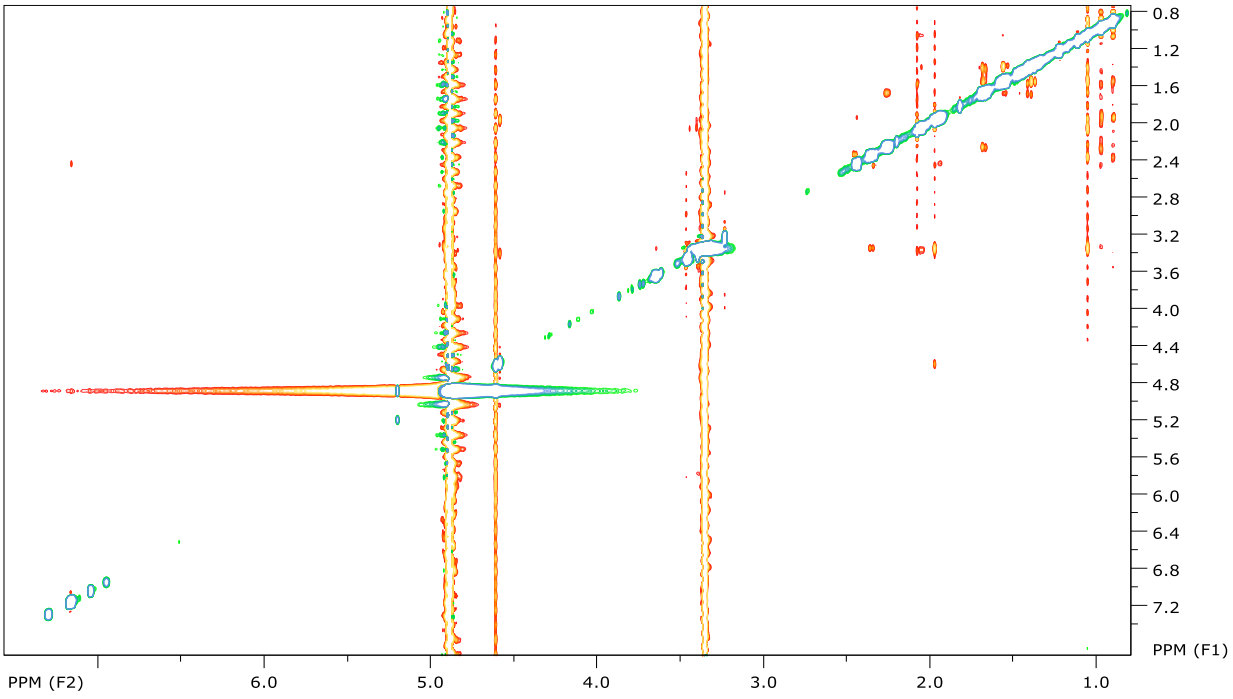

Fig S5. HSQC spectrum of brachialactone in MeOH-$_{d4}$ at 600 MHz.

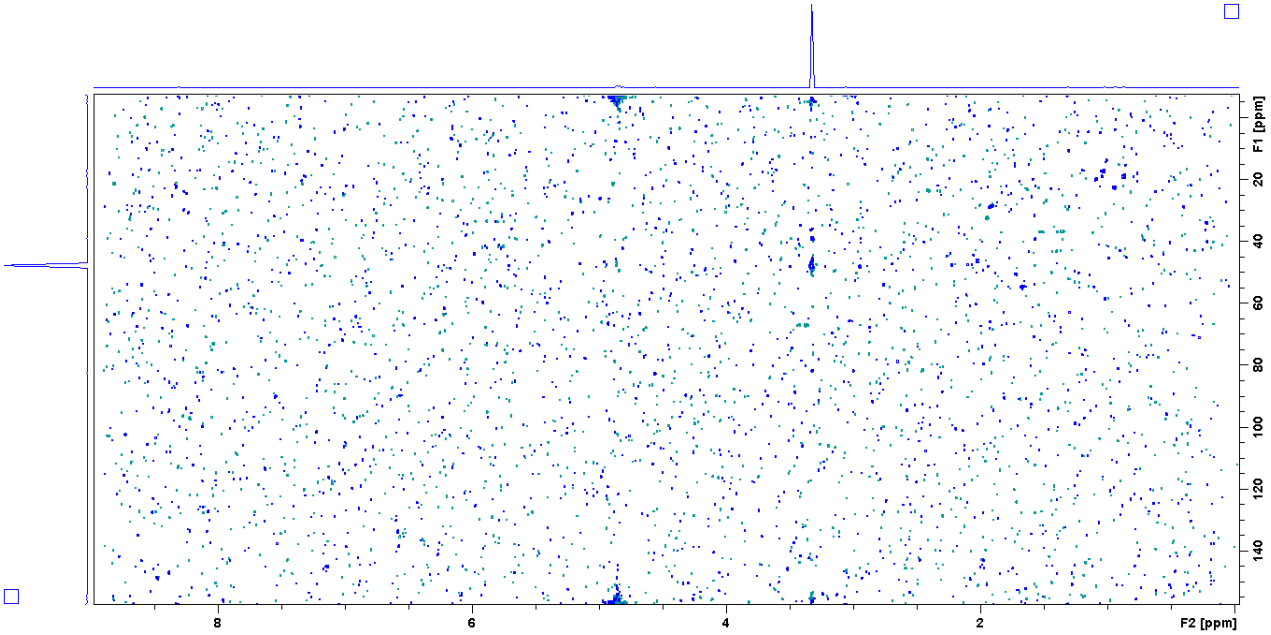

Fig S6. HMBC spectrum of brachialactone in MeOH-$_{d4}$ at 600 MHz.

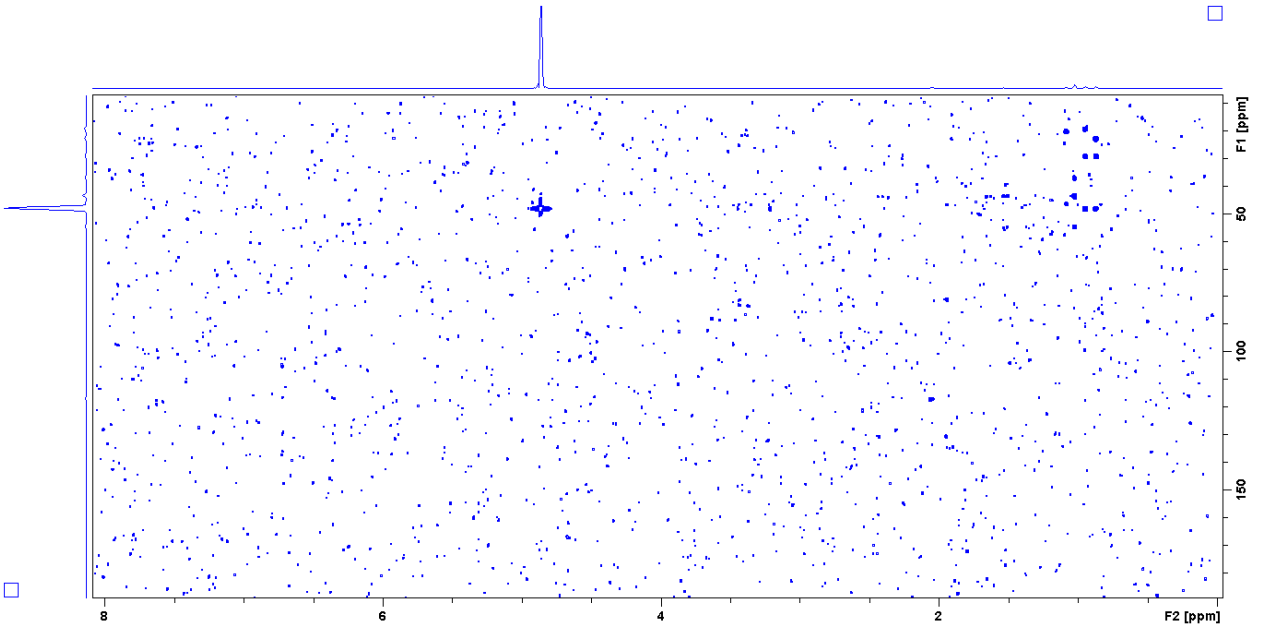

643 **Fig S7.** HRMS-spectrum of 3-*epi*-brachialactone

644

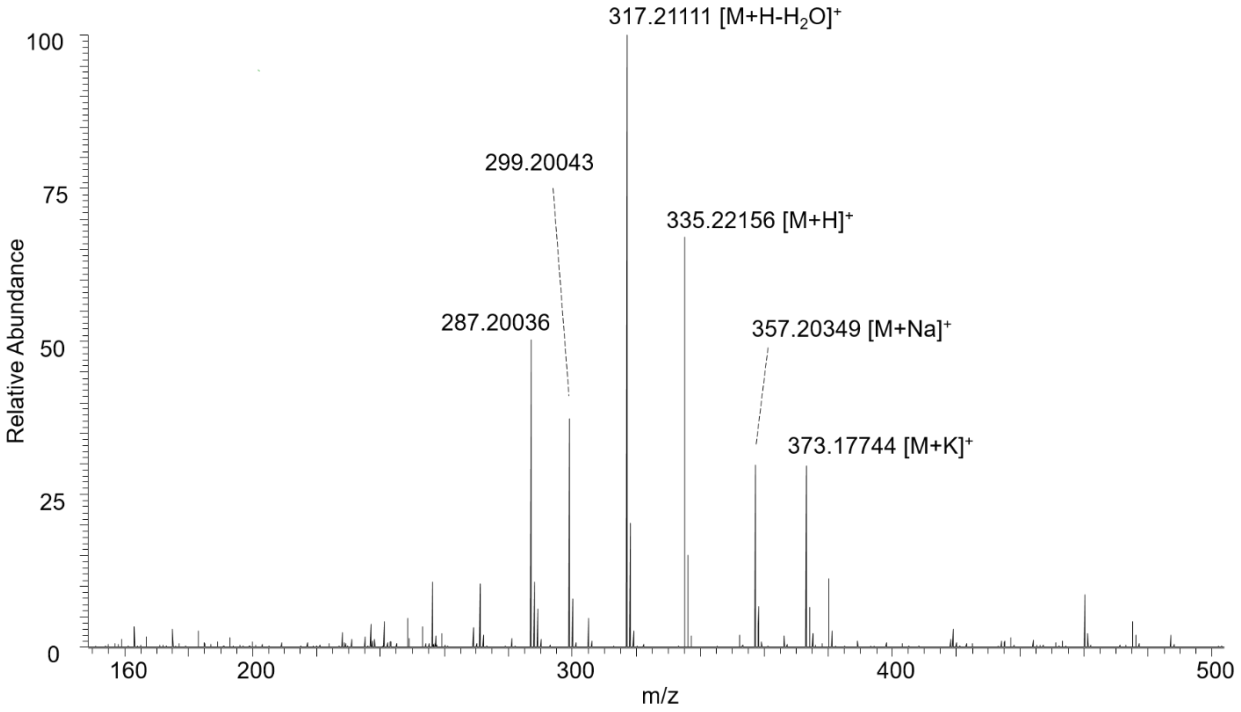

645

646

647 **Fig S8.** ^{1}H NMR spectrum of 3-*epi*-brachialactone in MeOH-$_{d4}$ at 600 MHz.

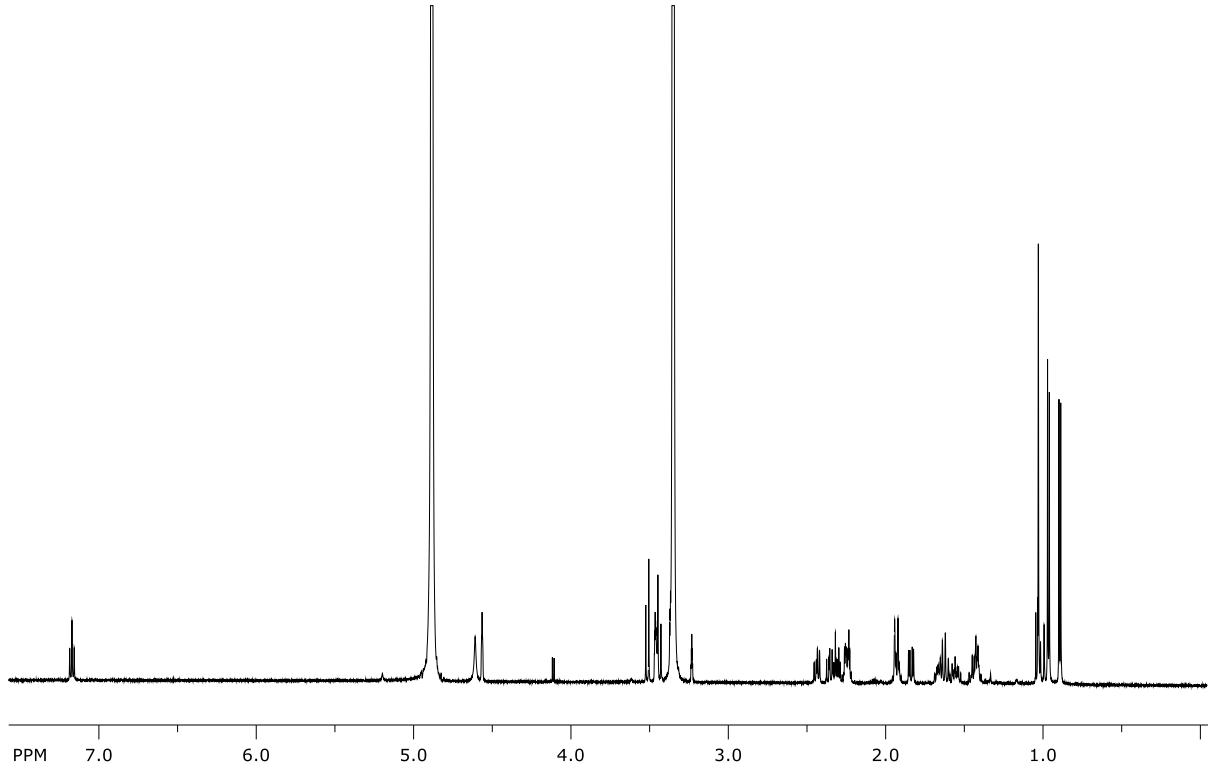

648

649

650

651

652

653

Fig S9. COSY spectrum of 3-*epi*-brachialactone in MeOH-$_{d4}$ at 600 MHz.

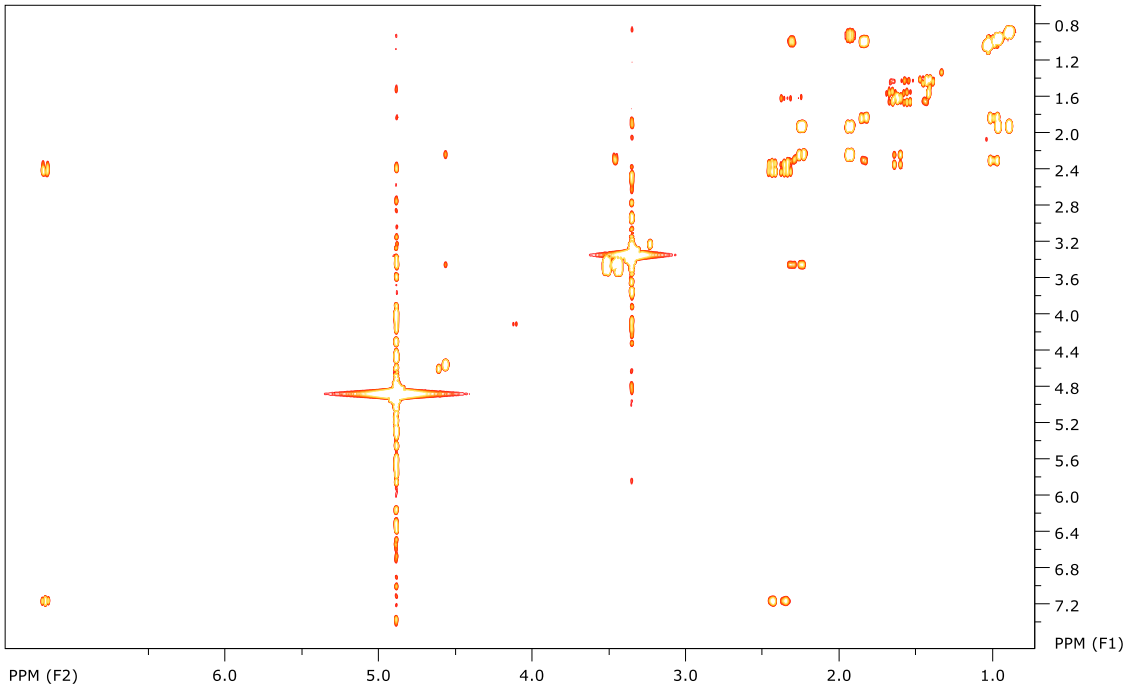

Fig S10. NOESY spectrum of 3-*epi*-brachialactone in MeOH-$_{d4}$ at 600 MHz.

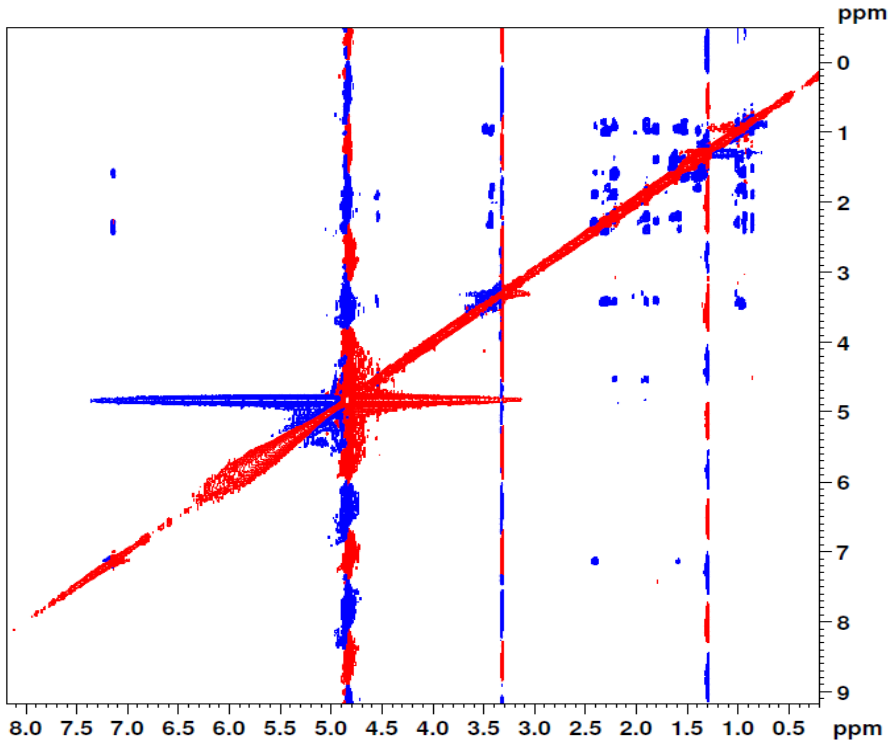

Fig S11. ^{13}C-NMR spectrum of 3-*epi*-brachialactone in MeOH-$_{d4}$ at 150 MHz.

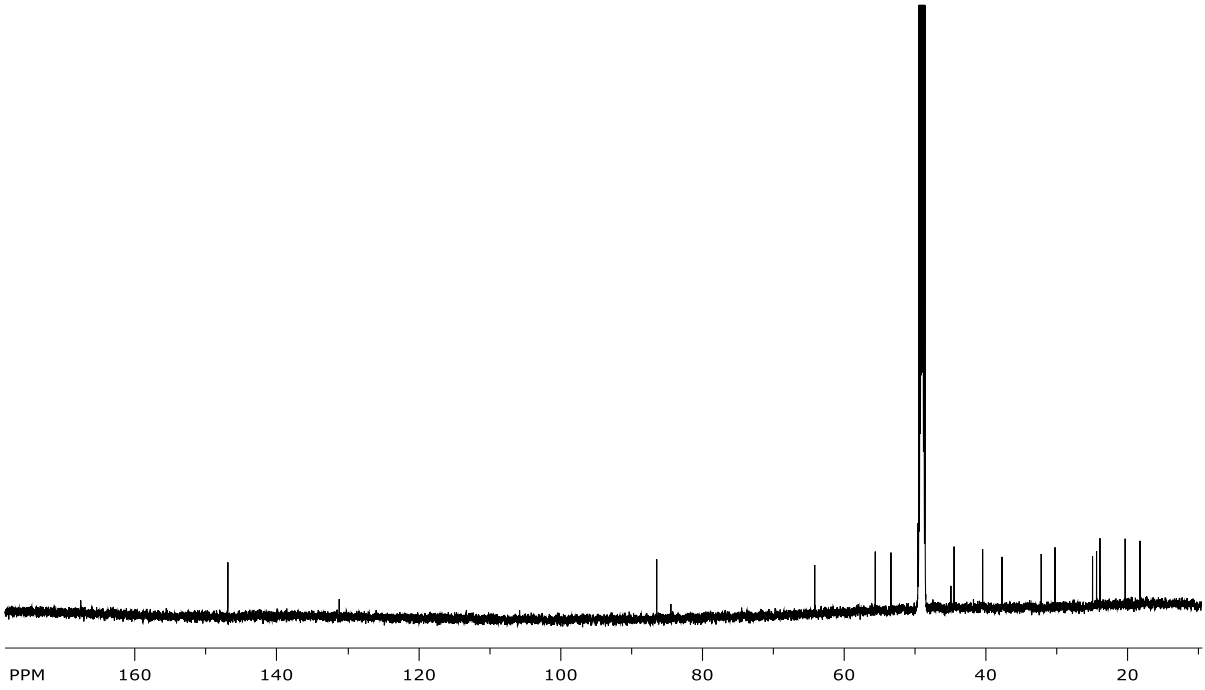

Fig S12. HSQC spectrum of 3-*epi*-brachialactone in MeOH-$_{d4}$ at 600 MHz.

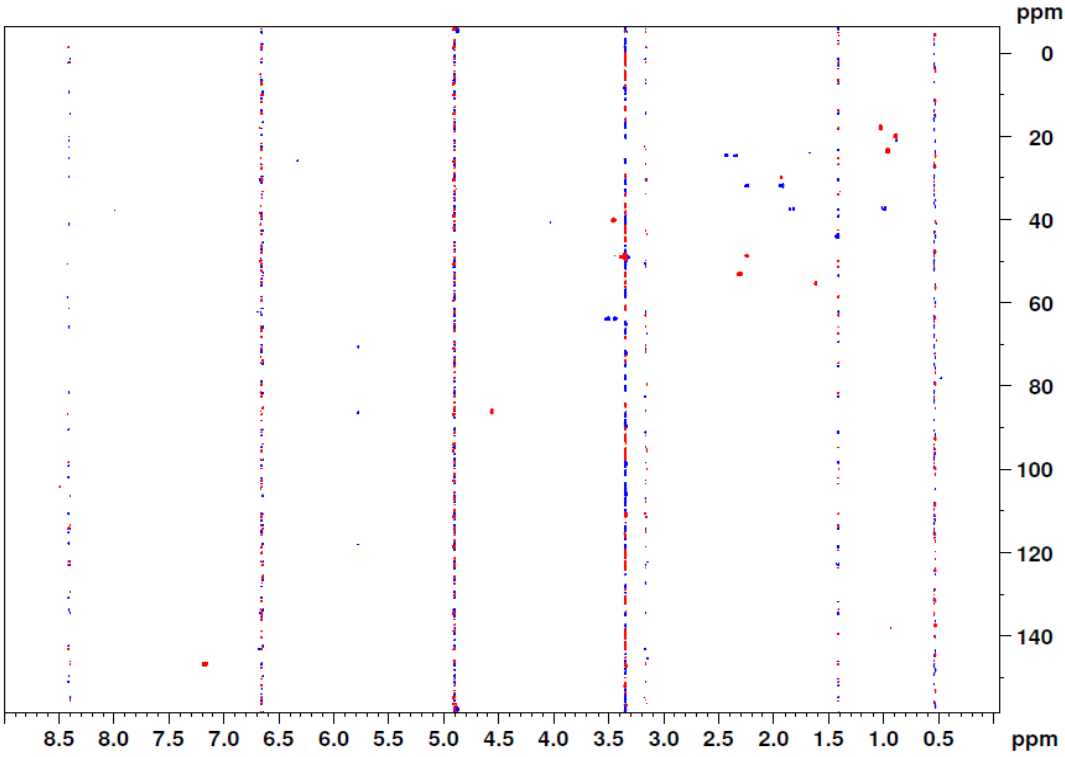

Fig S13. HMBC spectrum of 3-*epi*-brachialactone in MeOH-$_{d4}$ at 600 MHz.

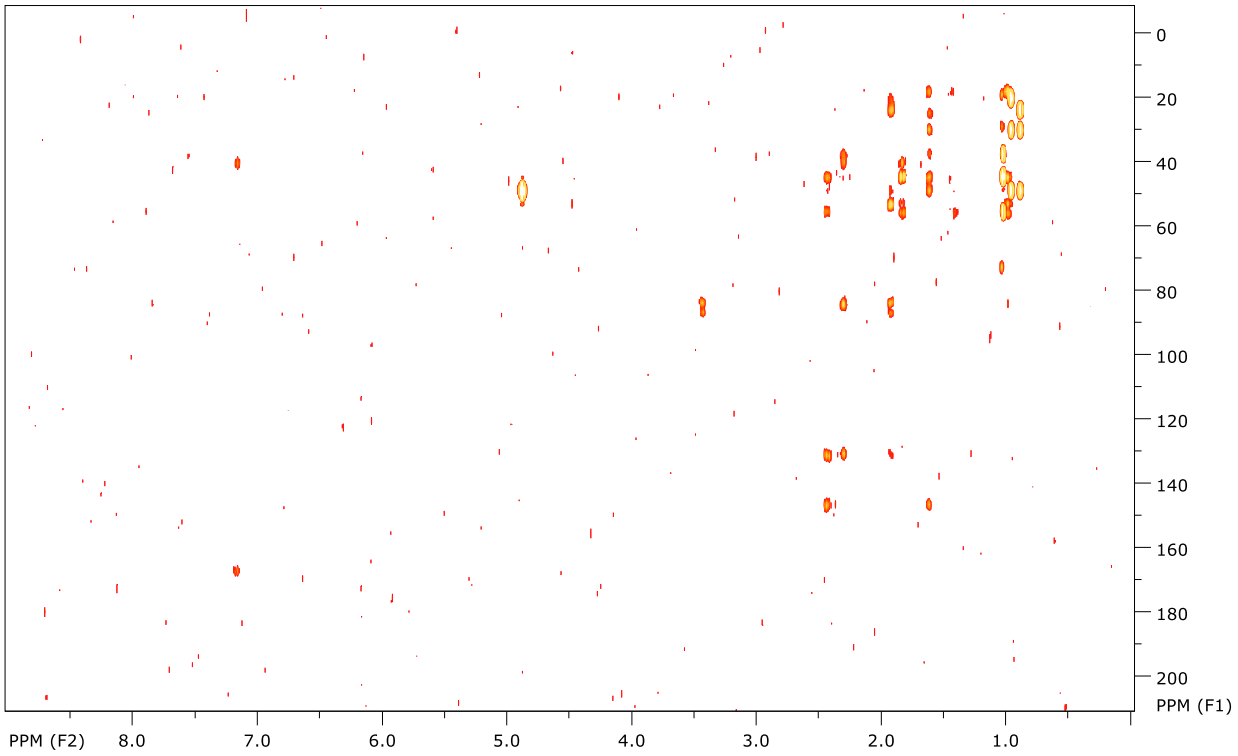

Fig S14. Selective HMBC spectrum of 3-*epi*-brachialactone in MeOH-$_{d4}$ at 600 MHz.

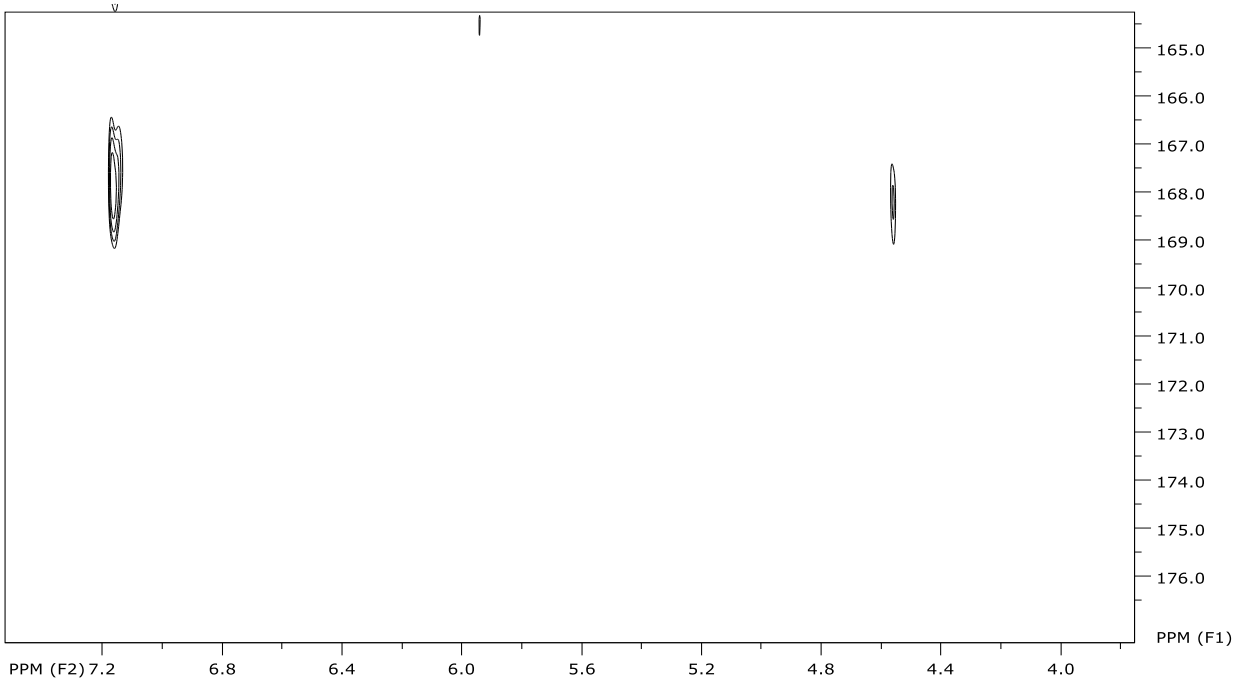

Fig S15. HRMS-spectrum of 16-hydroxy-3-*epi*-brachialactone

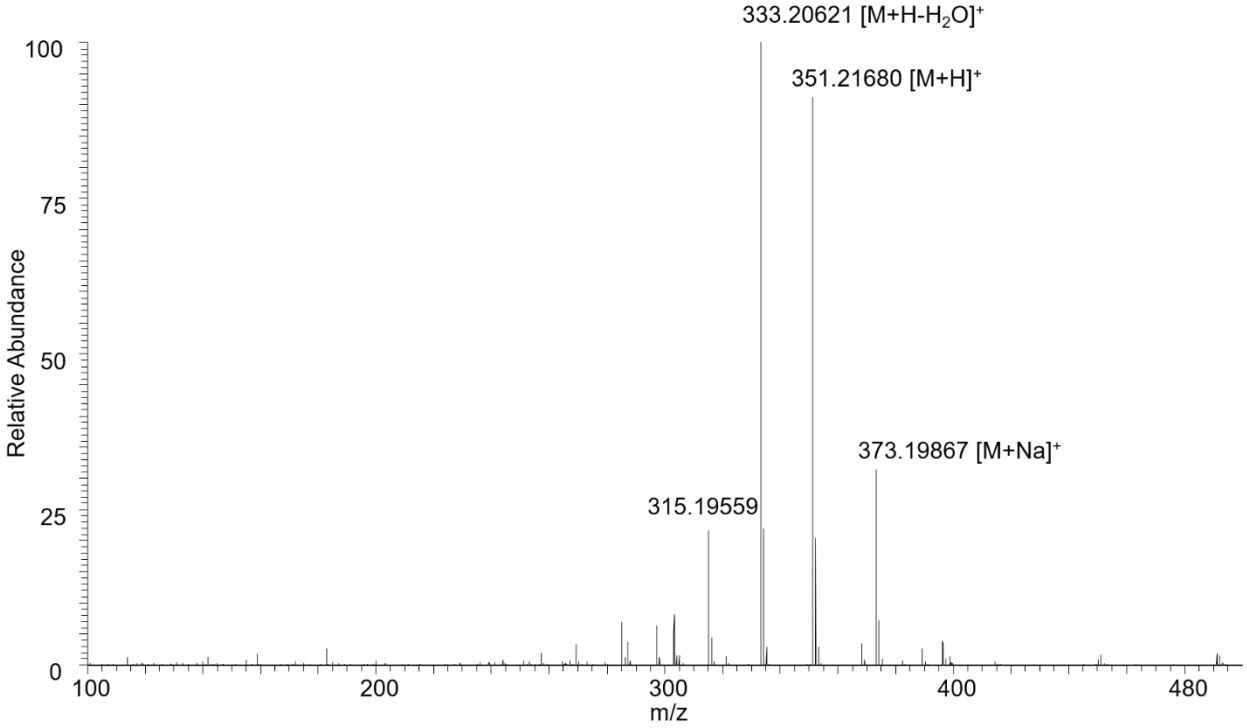

Fig S16. ^{1}H NMR spectrum of 16-hydroxy-3-*epi*-brachialactone in MeOH-$_{d4}$ at 600 MHz.

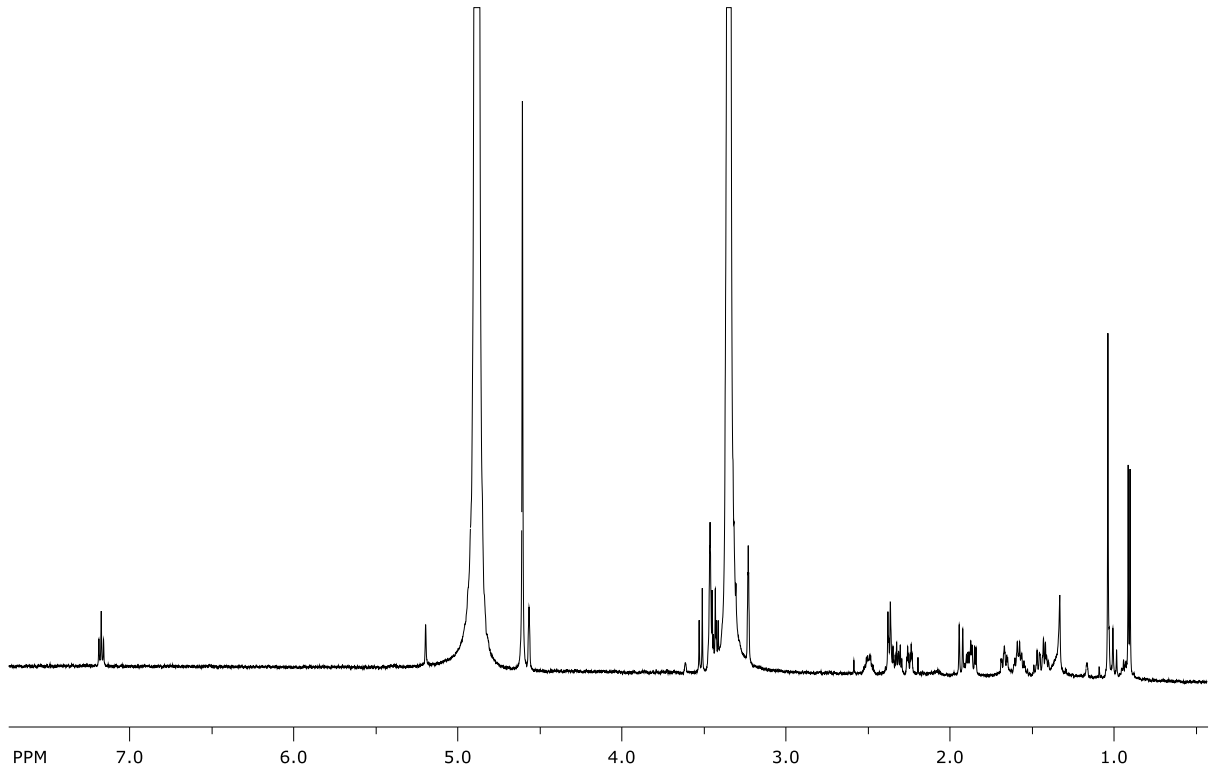

Fig S17. COSY spectrum of 16-hydroxy-3-*epi*-brachialactone in MeOH-$_{d4}$ at 600 MHz.

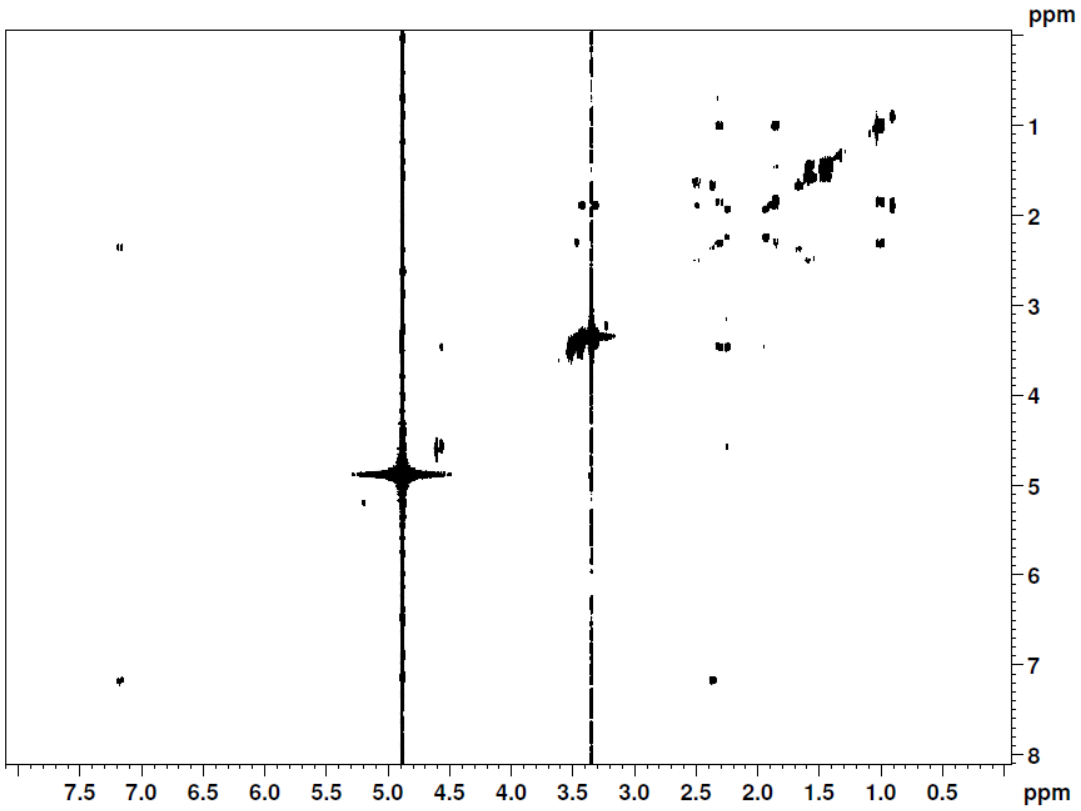

Fig S18. NOESY spectrum of 16-hydroxy-3-*epi*-brachialactone in MeOH-$_{d4}$ at 600 MHz.

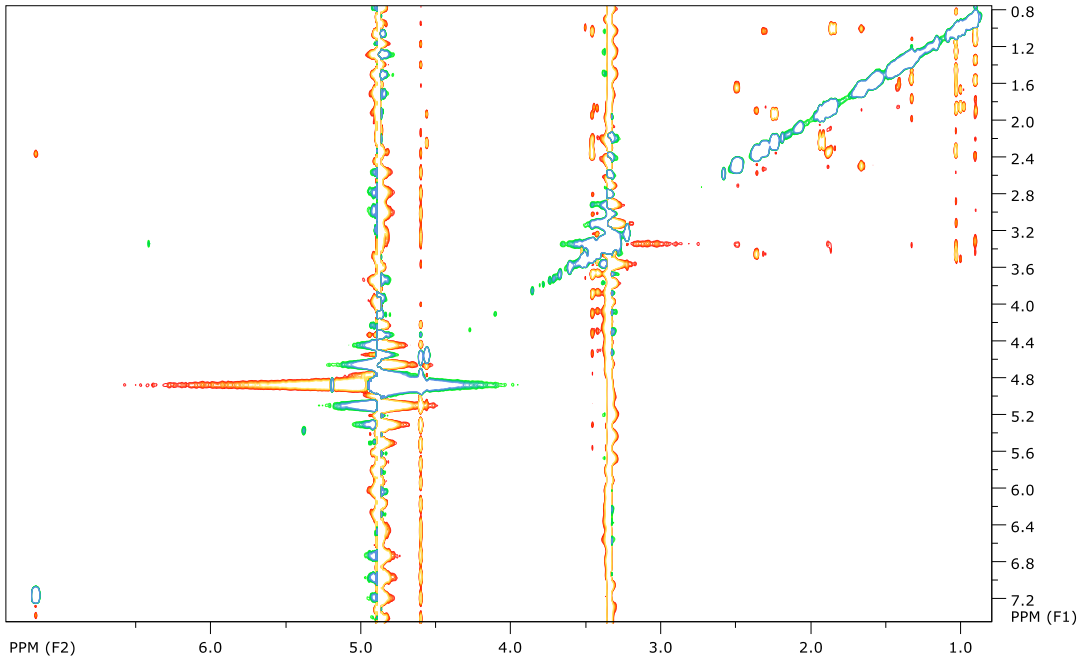

Fig S19. HSQC spectrum of 16-hydroxy-3-*epi*-brachialactone in MeOH-$_{d4}$ at 600 MHz.

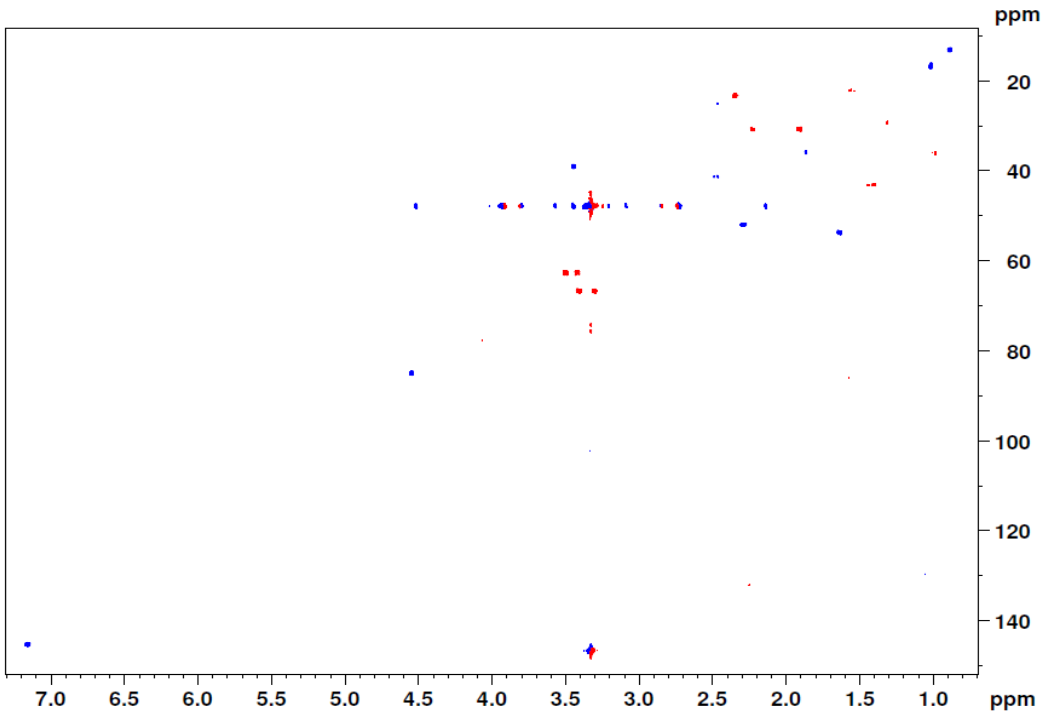

Fig S20. HMBC spectrum of 16-hydroxy-3-*epi*-brachialactone in MeOH-$_{d4}$ at 600 MHz.

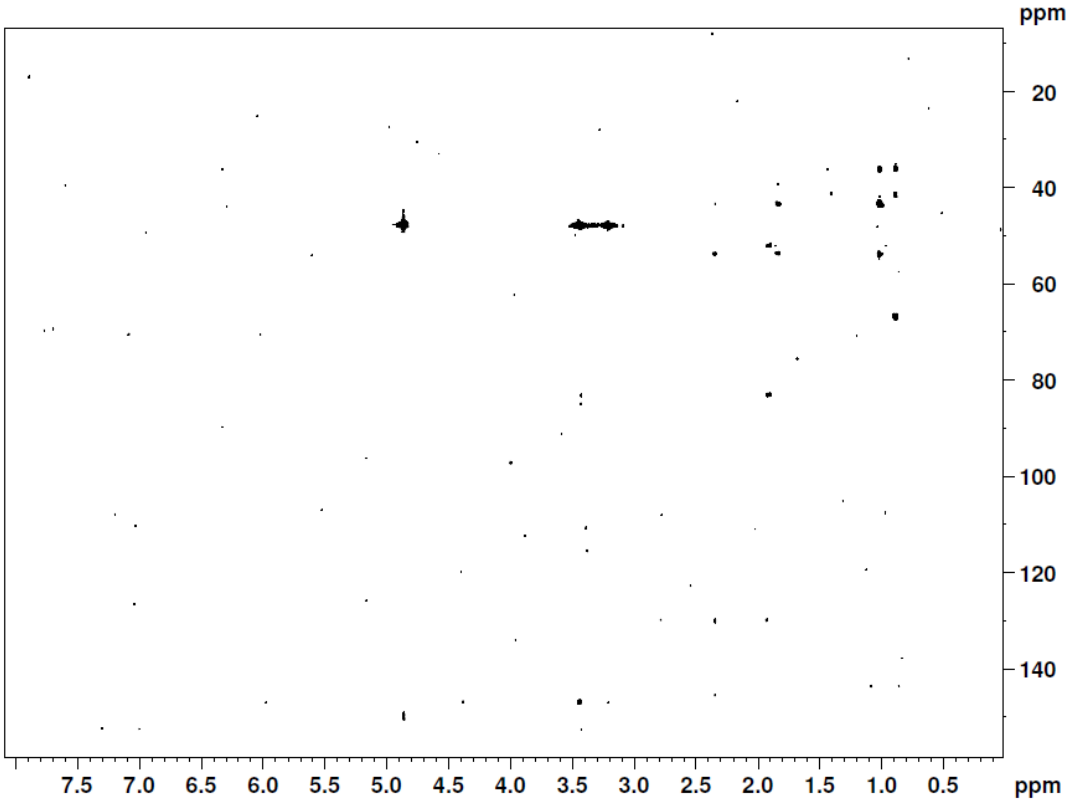

706 **Fig S21.** HRMS-spectrum of 3,18-epoxy-9-hydroxy-4,7-*seco*-brachialactone

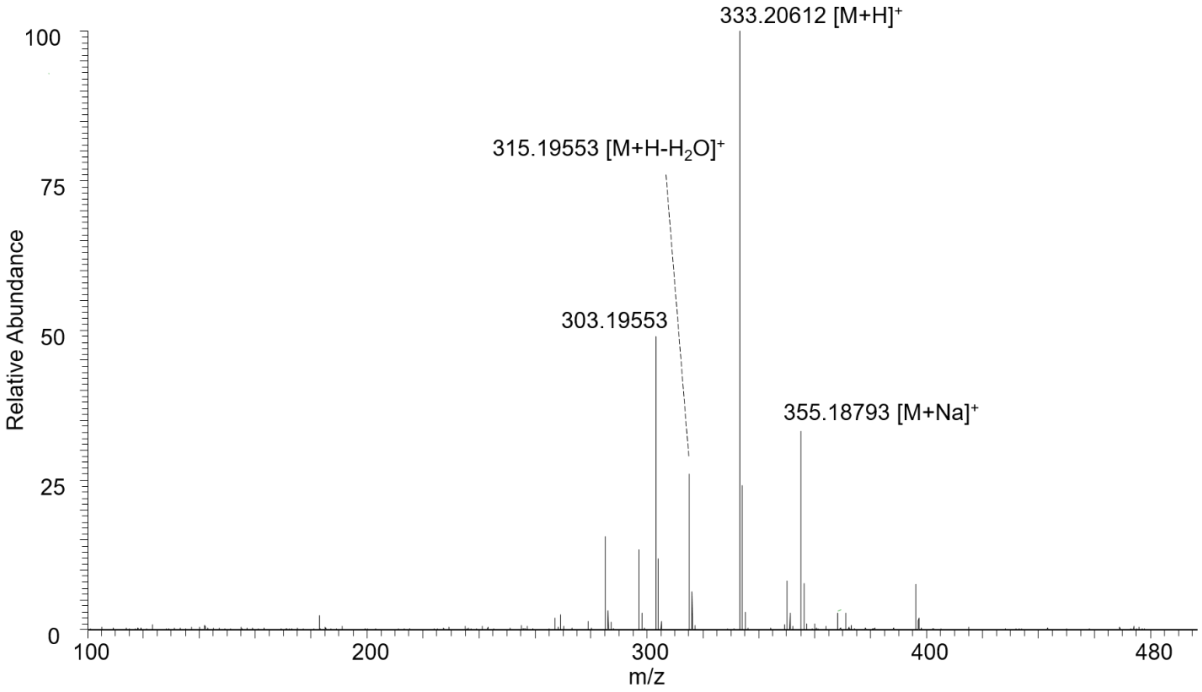

707
708
709 **Fig S22.** ^{1}H NMR spectrum of 3,18-epoxy-9-hydroxy-4,7-*seco*-brachialactone in MeOH-$_{d4}$ at
710 600 MHz.
711

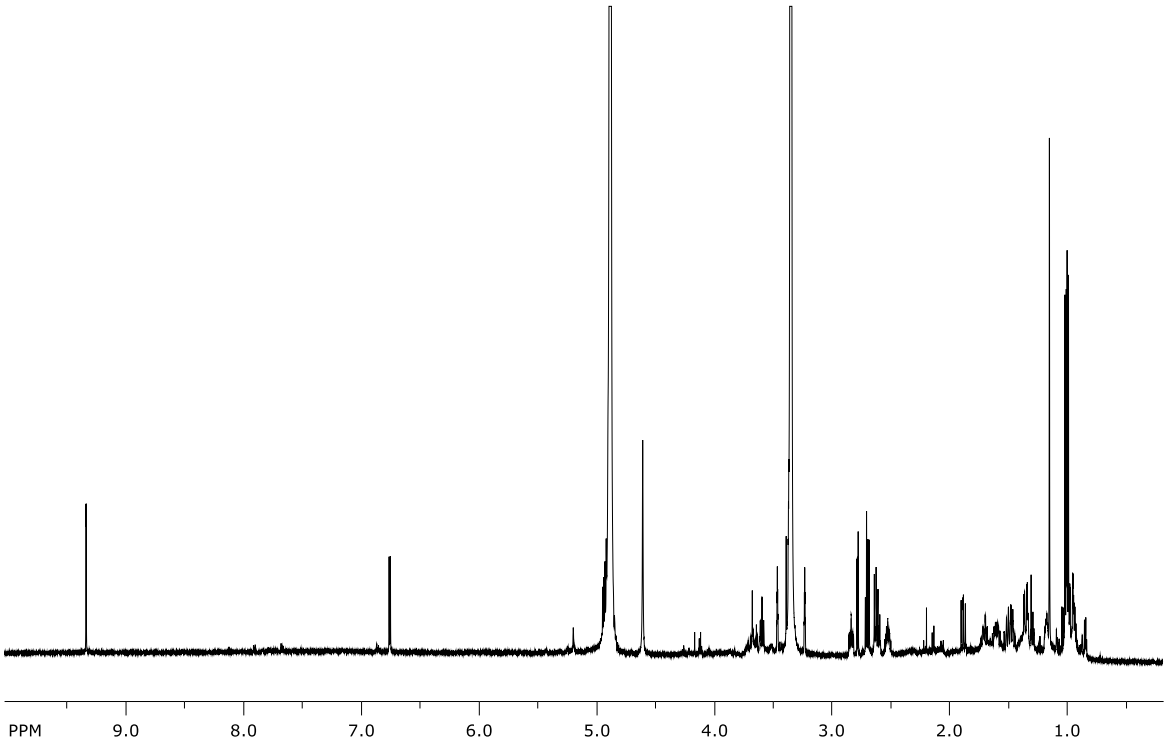

712

Fig S23. COSY spectrum of 3,18-epoxy-9-hydroxy-4,7-*seco*-brachialactone in MeOH-$_{d4}$ at 600 MHz.

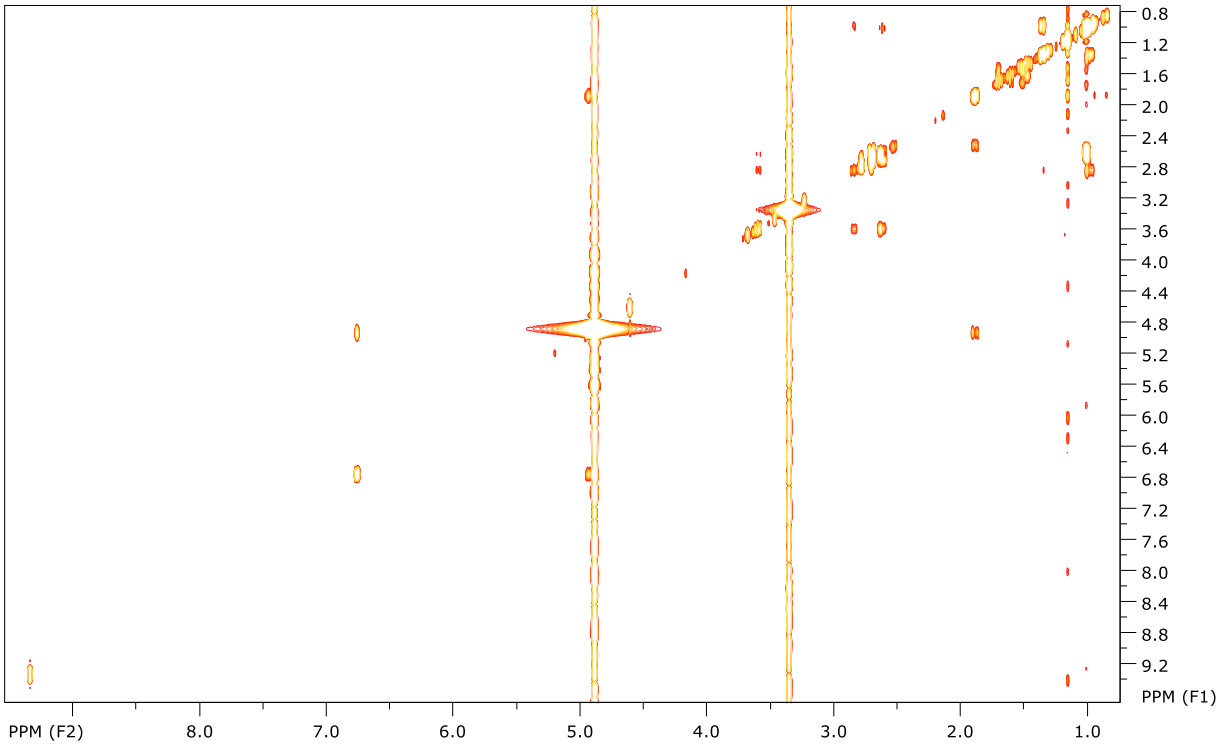

Fig S24. NOESY spectrum of 3,18-epoxy-9-hydroxy-4,7-*seco*-brachialactone in MeOH-$_{d4}$ at 600 MHz.

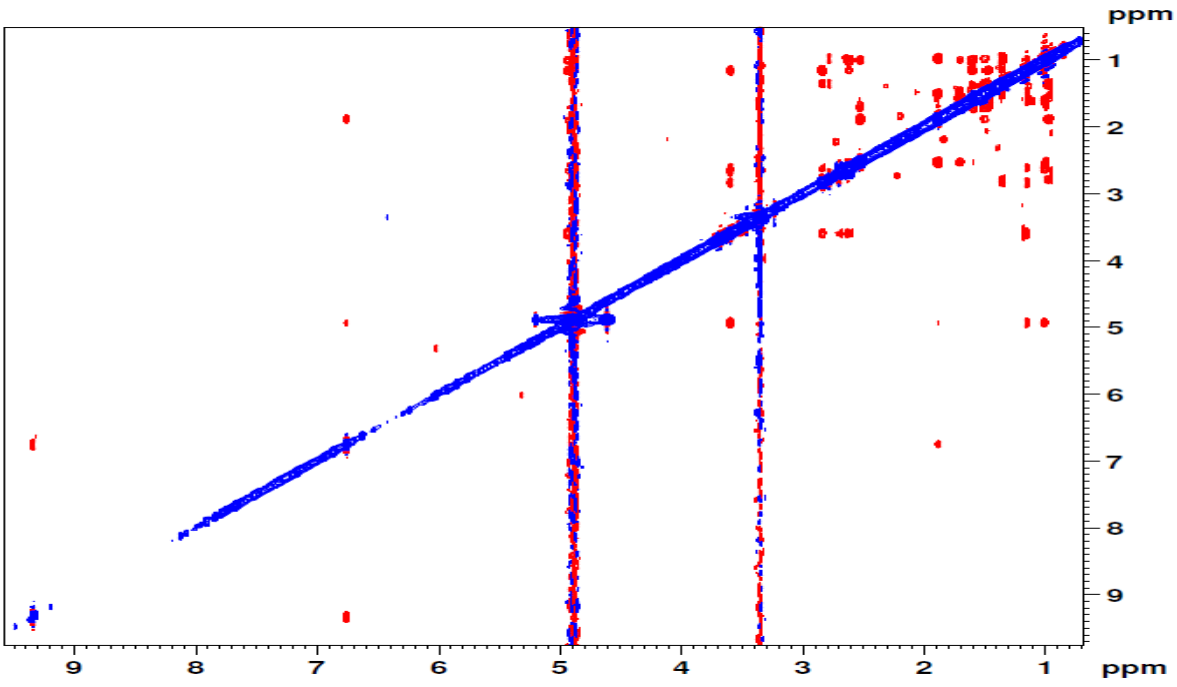

Fig S25. HSQC spectrum of 3,18-epoxy-9-hydroxy-4,7-*seco*-brachialactone in MeOH-$_{d4}$ at 600 MHz.

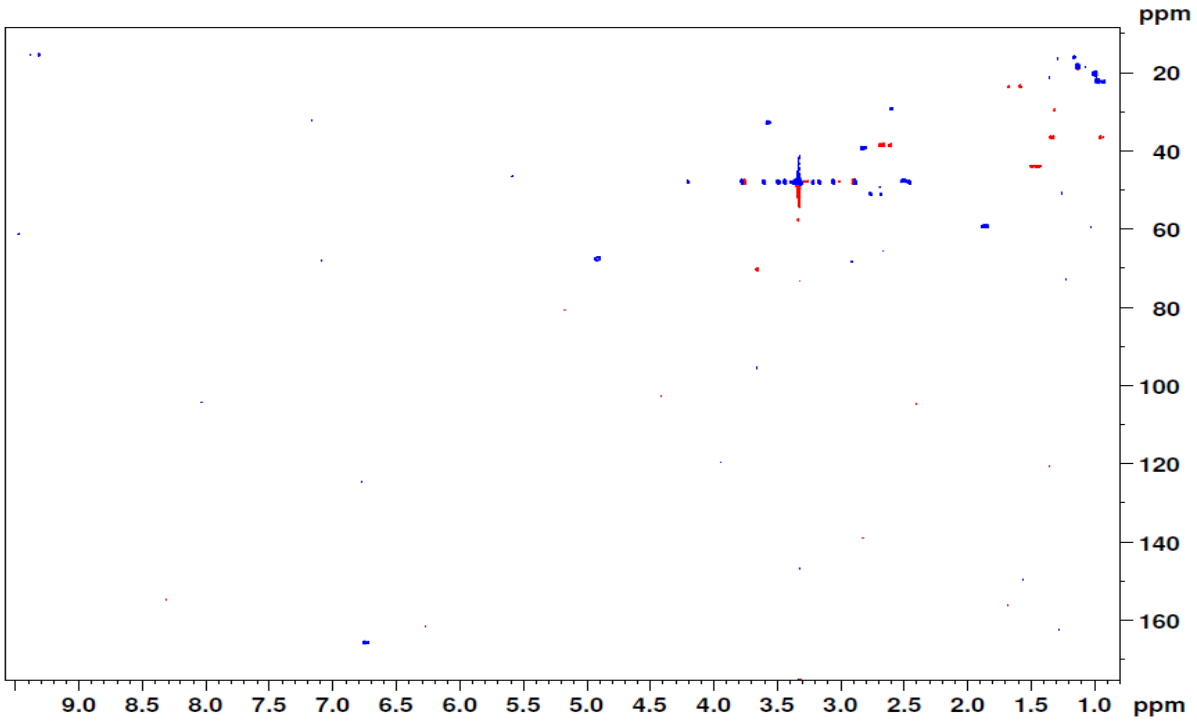

Fig S26. HMBC spectrum of 3,18-epoxy-9-hydroxy-4,7-*seco*-brachialactone in MeOH-$_{d4}$ at 600 MHz.

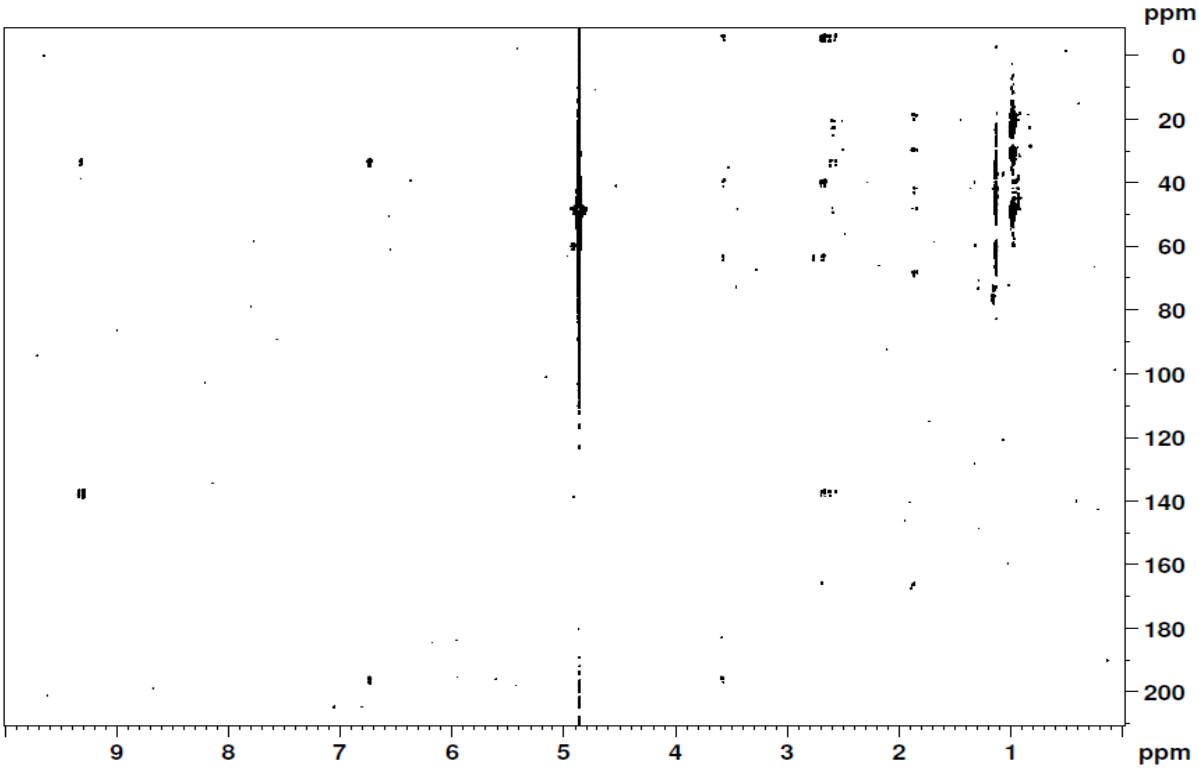

Fig. S27. Chemical structures of brachialactone (**1**) and 3-*epi*-brachialactone (**2**) isolated from the root exudates of *Brachiaria humidicola*. Both isomers differ in their absolute configuration at C3, as was proven by NOESY correlations. Important NOESY correlations displayed as continuous arrows, important HMBC as dashed arrows.

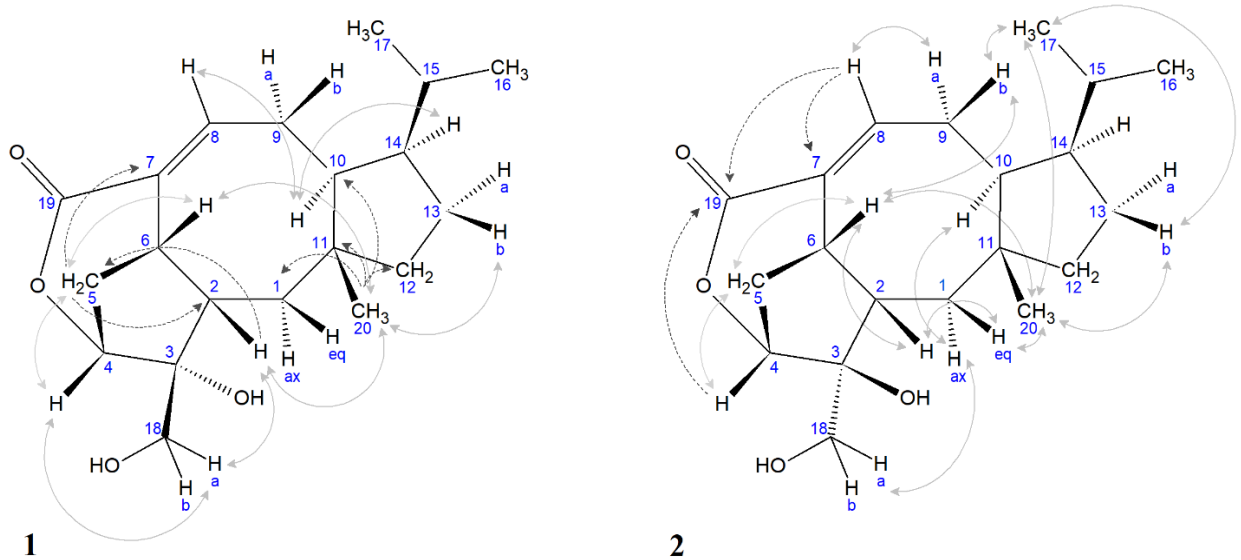

1 **2**

Fig. S28. Chemical structures of the brachialactone derivatives 16-hydroxy-3-*epi*-brachialactone (**3**) and 3,18-epoxy-9-hydroxy-4,7-*seco*-brachialactone (**4**) isolated from the root exudates of *Brachiaria humidicola*. Important NOESY correlations displayed as continuous arrows, important HMBC as dashed arrows.

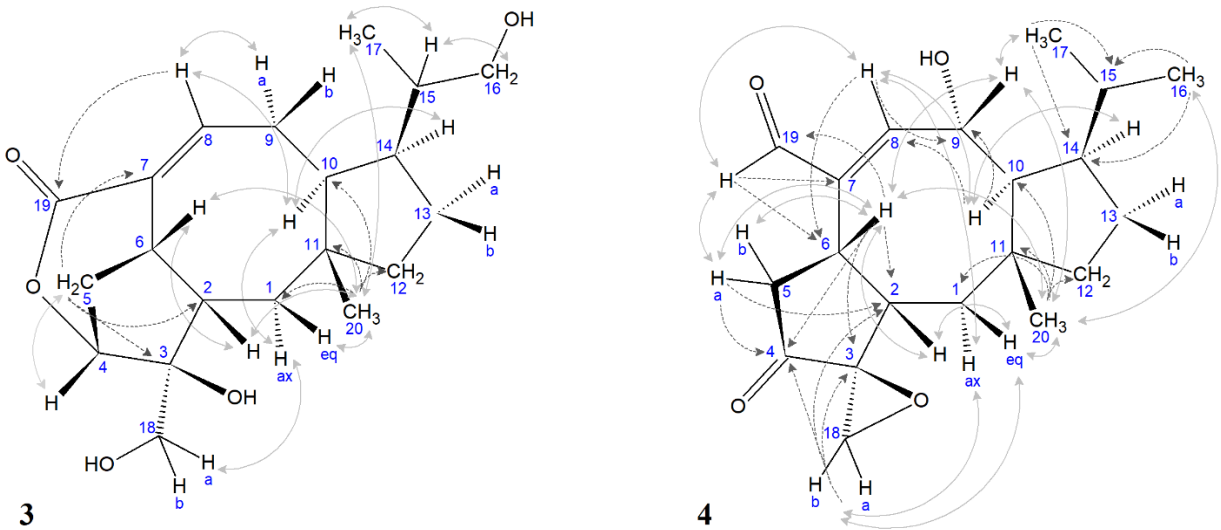

3 **4**

Fig S29. Structure and Cartesian coordinates of **2** of the DFT GIAO APDF/Aug-CC-pVTZ //APDF/6-311++G(2d,p) calculation**.**

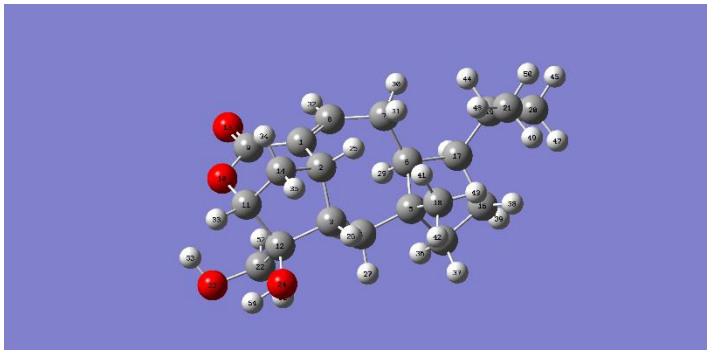

Center Number	Coordinates (Angstroms) X	Y	Z
1	-1.066626	1.555178	0.221431
2	-1.172174	0.513540	1.294541
3	-1.255528	-0.900594	0.677282
4	-0.224318	-1.284349	-0.383431
5	1.272951	-1.101537	-0.057971
6	1.838031	0.263775	-0.546231
7	1.440393	1.537154	0.220702
8	0.099285	2.012175	-0.237786
9	-2.314051	2.000757	-0.463057
10	-3.462366	1.342065	-0.135905
11	-3.416726	0.261473	0.820508
12	-2.743569	-1.012481	0.225159
13	-2.369783	2.871755	-1.290550
14	-2.526122	0.632579	1.983643
15	2.104809	-2.038919	-0.950877
16	3.525113	-1.479358	-0.906510
17	3.357477	0.054539	-0.845495
18	1.563553	-1.449211	1.402527
19	4.400751	0.788950	0.012707
20	5.795129	0.569829	-0.574748
21	4.411243	0.451088	1.500525
22	-2.975571	-1.100332	-1.282044
23	-4.364650	-1.130022	-1.567147
24	-3.306543	-2.160271	0.847156
25	-0.334018	0.604537	1.984892
26	-1.166902	-1.606578	1.510321
27	-0.388510	-2.346554	-0.602415
28	-0.419965	-0.749206	-1.317662
29	1.386822	0.376919	-1.540608
30	2.177420	2.320499	0.027342
31	1.450477	1.361884	1.299522
32	0.065348	2.721848	-1.061363
33	-4.460540	0.076885	1.071059
34	-2.744246	1.626214	2.381563
35	-2.629367	-0.105086	2.783083
36	1.712803	-1.997130	-1.974663
37	2.039603	-3.081288	-0.623924
38	4.045550	-1.844963	-0.016524
39	4.125037	-1.797407	-1.762175
40	3.516422	0.448737	-1.856760
41	1.179961	-0.711862	2.108954
42	1.098369	-2.408219	1.650128
43	2.631057	-1.550636	1.590036
44	4.182196	1.861864	-0.073786
45	6.544694	1.159715	-0.039991
46	5.836325	0.852211	-1.630839
47	6.091917	-0.480962	-0.500788
48	3.445242	0.621855	1.976772
49	4.695401	-0.590164	1.678823
50	5.148053	1.071496	2.019021
51	-2.564138	-2.042497	-1.649330
52	-2.482769	-0.283779	-1.816583
53	-4.686257	-0.223006	-1.517934
54	-4.153554	-2.319086	0.410144

Fig S30. Structure and Cartesian coordinates of **1a** of the DFT GIAO APDF/Aug-CC-pVTZ //APDF/6-311++G(2d,p) calculation**.**

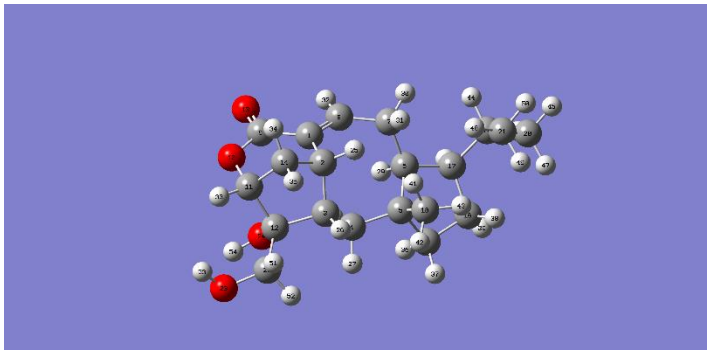

Center Number	Coordinates (Angstroms) X	Y	Z
1	-0.994450	1.650493	0.185626
2	-1.185348	0.569987	1.208615
3	-1.299985	-0.804284	0.518769
4	-0.248632	-1.188261	-0.519204
5	1.239448	-1.092233	-0.128672
6	1.882359	0.266823	-0.529660
7	1.508685	1.518558	0.282838
8	0.208098	2.073370	-0.203490
9	-2.194472	2.191540	-0.518791
10	-3.387487	1.593431	-0.251827
11	-3.415956	0.454833	0.610742
12	-2.751017	-0.795896	-0.055578
13	-2.171825	3.117874	-1.283957
14	-2.565190	0.710628	1.840226
15	2.064146	-2.024248	-1.033773
16	3.504890	-1.532208	-0.910897
17	3.401545	0.003353	-0.783088
18	1.460030	-1.518808	1.323395
19	4.442182	0.650454	0.145700
20	5.847545	0.394696	-0.399219
21	4.380297	0.246680	1.615763
22	-3.493246	-2.069942	0.342406
23	-4.728237	-2.199612	-0.343523
24	-2.730138	-0.694471	-1.456289
25	-0.378164	0.597804	1.940635
26	-1.279555	-1.551719	1.324385
27	-0.458337	-2.226917	-0.803464
28	-0.409666	-0.604139	-1.427425
29	1.473798	0.445664	-1.532271
30	2.285262	2.277194	0.156535
31	1.469043	1.293010	1.351873
32	0.237703	2.818717	-0.994954
33	-4.479120	0.310971	0.817045
34	-2.764057	1.689796	2.281412
35	-2.730852	-0.056955	2.602161
36	1.713026	-1.917635	-2.067317
37	1.941646	-3.076871	-0.759651
38	3.974661	-1.961477	-0.020925
39	4.123094	-1.837385	-1.758304
40	3.616135	0.435593	-1.768204
41	1.076373	-0.800520	2.049535
42	0.950478	-2.470234	1.506411
43	2.514488	-1.670871	1.547417
44	4.273811	1.734916	0.101187
45	6.601045	0.925361	0.189491
46	5.941886	0.721661	-1.438905
47	6.094750	-0.670866	-0.363354
48	3.404958	0.440721	2.063308
49	4.610695	-0.813623	1.755792
50	5.123410	0.808625	2.189197
51	-3.629435	-2.113734	1.430964
52	-2.892777	-2.932316	0.042016
53	-5.390949	-1.653943	0.088116
54	-3.617417	-0.911819	-1.768194

Fig S31. Structure and Cartesian coordinates of **1b** of the DFT GIAO APDF/Aug-CC-pVTZ //APDF/6-311++G(2d,p) calculation**.**

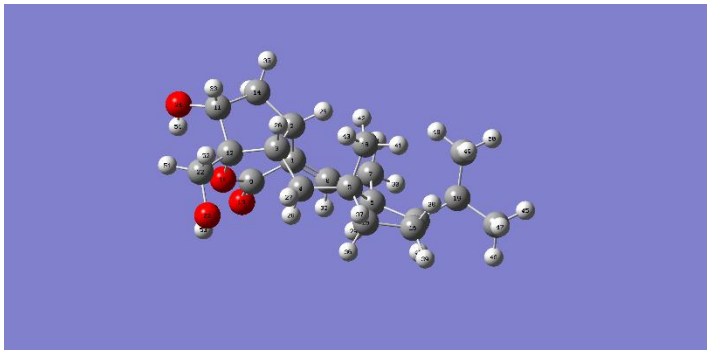

Center Number	Coordinates (Angstroms) X	Y	Z
1	1.023526	-1.534338	-0.306247
2	1.173280	-0.903287	1.037946
3	1.315729	0.602122	0.744778
4	0.263210	1.249592	-0.157774
5	-1.227350	1.005949	0.177637
6	-1.865637	-0.194808	-0.588188
7	-1.469637	-1.633480	-0.198737
8	-0.143402	-1.905020	-0.832455
9	2.157819	-1.331900	-1.238549
10	2.916218	-0.215328	-0.980585
11	3.498809	-0.160861	1.343364
12	2.756062	0.590424	0.226577
13	2.417483	-1.984863	-2.211139
14	2.499221	-1.278025	1.730268
15	-2.070385	2.142089	-0.429672
16	-3.506140	1.619238	-0.439326
17	-3.389876	0.108422	-0.737204
18	-1.450608	1.013845	1.691753
19	-4.406209	-0.783629	-0.004965
20	-5.823152	-0.412734	-0.443276
21	-4.326635	-0.793887	1.518560
22	3.392107	1.919505	-0.124312
23	2.848427	2.512659	-1.281150
24	4.784453	-0.593231	0.982477
25	0.314853	-1.139685	1.661353
26	1.347274	1.141564	1.700314
27	0.445660	2.328397	-0.128315
28	0.440376	0.962681	-1.198285
29	-1.474871	-0.063876	-1.606250
30	-2.215906	-2.333163	-0.583833
31	-1.445811	-1.764204	0.885187
32	-0.145727	-2.238320	-1.868118
33	3.650220	0.526715	2.181086
34	2.874540	-2.248362	1.394861
35	2.378873	-1.343329	2.813664
36	-1.727412	2.332467	-1.453821
37	-1.955325	3.078043	0.125611
38	-3.973401	1.784089	0.536008
39	-4.132408	2.138541	-1.168190
40	-3.618601	-0.042423	-1.799459
41	-2.504905	1.108663	1.944566
42	-1.079092	0.119673	2.193563
43	-0.935701	1.873243	2.132489
44	-4.223915	-1.812234	-0.344311
45	-6.560752	-1.093793	-0.009801
46	-5.930795	-0.449253	-1.531319
47	-6.081872	0.599895	-0.118577
48	-3.341977	-1.085075	1.885999
49	-4.570070	0.183770	1.944836
50	-5.052670	-1.504007	1.925089
51	4.475578	1.772121	-0.221132
52	3.222215	2.617960	0.699326
53	2.962551	1.883988	-2.001808
54	4.722025	-1.003272	0.111368

Table S5. Computational studies. Calculated and experimental ^{13}C NMR data of **2**, **1** with a C4-O-C19 (=**1a**) and **1** with a C3-O-C19 (=**1b**) lactone.

	2		**1a**		**1b**
Carbon No	Calc. δ (ppm)	Exp. δ (ppm)	Calc. δ (ppm)	Exp. δ (ppm)	Calc. δ (ppm)
1	39.9	37.4	40.3	37.9	41.8
2	54.5	53.4	51.9	47.5	51.7
3	88.4	84.0	84.4	82.0	93.7
4	89.2	86.4	82.7	83.7	79.9
5	33.9	32.1	36.3	33.4	39.4
6	44.4	40.4	43.9	40.1	41.4
11	47.4	44.9	46.9	44.5	48.6
18	70.2	64.1	71.4	68.1	67.6
19	168.0	168.0	167.7	-	171.0

Theoretical ^{13}C NMR chemical shifts (δ_a) were derived by the following equation:

$\delta_a = \sigma_{ref} - \sigma_a + \delta_{ref}$

where σ_{ref} and σ_a are the calculated NMR isotropic magnetic shielding tensors of the reference compound and carbon a of the compound of interest: σ_{TMS} = 188.7 ppm . δ_{ref} represents the chemical shift of the reference compound (=0 ppm for TMS).

Fig. S32. Relative activity of *Nitrosomonas europaea* cultures: Pure culture, DMSO (0.45%) and allylthiourea (ED_{50} and ED_{80}) controls. Bars represent untreated pure culture, a DMSO (0.45%) treatment that served as blank for the assessment of the nitrification inhibiting activity of tested BL compounds and a control with the synthetic nitrification inhibitor Allylthiourea (AT) at effective dosages 50 (0.1 µM) and 80 (0.22 µM).